Bimodal back-arc alkaline magmatism after ridge subduction: Pliocene felsic rocks from Central Patagonia (47°S)

Felipe Espinoza [a,*], Diego Morata [a], Mireille Polvé [b], Yves Lagabrielle [c], René C. Maury [d], Christèle Guivel [e], Joseph Cotten [d], Hervé Bellon [d], Manuel Suárez [f]

[a] *Departamento de Geología, Universidad de Chile, Casilla 13518, Correo 21, Santiago, Chile*
[b] *LMTG, Université de Toulouse, CNRS, IRD, OMP Avenue E.douard Belin 31400 Toulouse, France*
[c] *UMR 5243 Géosciences Montpellier, Université de Montpellier 2, Place Eugène Bataillon, CC 60, 34095 Montpellier Cedex 5, France*
[d] *UMR 6538 Domaines océaniques, Université de Bretagne Occidentale, 6 avenue le Gorgeu, C.S. 93837, 29238 Brest Cedex 3, France*
[e] *UMR 6112 Laboratoire de Planétologie et Géodynamique, Pétrologie Structurale, Université de Nantes, 2 rue de la Houssinière, B. P. 92208, 44322 Nantes Cedex 03, France*
[f] *Servicio Nacional de Geología y Minería, Avenida Santa María 0104, Santiago, Chile*

Abstract

Volumetrically minor microsyenites, alkali microgranite and related trachytic dykes intrude early Pliocene OIB-like alkali basaltic and basanitic flows of the Meseta del Lago Buenos Aires in Central Patagonia (47°S–71°30′W), and occur together with scarce trachytic lava flows. Whole-rock K–Ar ages between 3.98 and 3.08 Ma indicate that the emplacement of these felsic rocks occurred more or less synchronously with that of the post-plateau basaltic sequence that they intrude, during a bimodal mafic–felsic magmatic episode devoid of intermediate compositions. Chemically, these rocks have A_1-type granitoid affinities and are characterized by high silica and alkali contents (60–68 wt.% SiO_2; 8.7–10.8 wt.% Na_2O+K_2O), major and trace elements patterns evidencing evolution by low-pressure fractional crystallization, and Sr and Nd isotopic signatures similar to those of coeval basalts ($(^{87}Sr/^{86}Sr)_o$=0.70488–0.70571; $(^{143}Nd/^{144}Nd)_o$=0.512603–0.512645). Nevertheless, some of them have the most radiogenic Sr values ever reported for a magmatic rock in the Meseta and even in the whole Neogene Patagonian Plateau Lavas province ($(^{87}Sr/^{86}Sr)_o$=0.70556–0.70571; $(^{143}Nd/^{144}Nd)_o$=0.512603–0.512608). In addition, very high contents of strongly incompatible elements in the most evolved rocks, together with Sr isotopic ratios higher than those of coeval basalts, suggest the occurrence of open-system magmatic processes. Continuous fractional crystallization from a primitive basaltic source, similar to post-plateau coeval basalts, towards alkali granites combined with small rates of assimilation of host Jurassic tuffs (AFC) in a shallow magmatic reservoir, best explains the geochemical and petrographic features of the felsic rocks. Therefore, A_1-type magmatic rocks can be generated by open-system crystallization of deep asthenospheric melts in back-arc tectonic settings.

In Central Patagonia, these ~3–4 Ma old alkaline intrusions occur aligned along a ~N160–170 trending lineament, the Zeballos Fault Zone, stacking the morphotectonic front of one segment of the Patagonian Cordillera. Intrusion along this fault zone

* Corresponding author. Present address: Servicio Nacional de Geología y Minería, Avenida Santa María 0104, Santiago, Chile. Fax: +56 2 7372026.
E-mail address: fespinoza@sernageomin.cl (F. Espinoza).

occurred during the onset of a new transtensional or extensional event in the area, related to major regional tectonics occurring in possible relation with the collision of one segment of the Chile Spreading Ridge with the trench.

Keywords: Mafic–felsic alkaline magmatism; Syenites; Central Patagonia back-arc; Pliocene; Chemical modeling

1. Introduction

Alkaline bimodal (mafic–felsic) magmatism is typically found in extensional tectonic settings such as continental rifting zones (e.g. Trua et al., 1999; Ayalew and Yirgu, 2003; Peccerillo et al., 2003) and back-arc basins (e.g. Shinjo and Kato, 2000). In these settings, basalts represent huge volumes of flood lava flows (OIB-like signatures) associated in space and time with variable amounts of felsic volcanic rocks. The genesis of mafic volcanism is usually related to mantle upwelling with variable participation of the asthenosphere and the lithosphere to the source of the magmas. Genetic models explaining the relationships between silica-undersaturated mafic and silica-oversaturated felsic magmas (with absence of intermediate compositions) are still a matter of debate. Some workers have proposed that the alkaline felsic melts are generated from partial melting of crustal rocks (anatexis) or young underplated basalts (Whalen et al., 1987; Tchameni et al., 2001), while the mafic lavas derive directly from partial melting of mantle rocks. However, fractionation of mantle-derived mafic magmas, occurring in open-system conditions (e.g. associated with partial melting of crustal rocks, assimilation of crust coupled with fractional crystallization – AFC – of basaltic magmas and magma mixing) seems to be a more viable mechanism to generate bimodal magmatic suites (Whalen et al., 1987; Mingram et al., 2000; Tchameni et al., 2001; Litvinovsky et al., 2002; Peccerillo et al., 2003; Vernikovsky et al., 2003; Wang et al., 2005).

The Meseta del Lago Buenos Aires (MLBA; 47°S–71°30′W) is one of the largest (~6000 km^2) most voluminous (ca. 2000 km^3) basaltic plateaus in the back-arc domain of Central Patagonia. It forms part of a regional-scale basaltic province named Neogene Patagonian Plateau Lavas (NPPL, Gorring et al., 1997) outcropping from 46°30′S to 52°S in Argentina (Fig. 1). This province has first been genetically and chronologically related to the development and northward migration of a series of slab windows opened as a consequence of the subduction of the South Chile Spreading Ridge (SCR) under the South American Plate since ~15 Ma (Cande and Leslie, 1986; Ramos and Kay, 1992; Gorring et al., 1997; Gorring and Kay, 2001). However, a recent chronological and petrogenetic study of the Miocene MLBA main-plateau basalts by Guivel et al. (2006) has shown that the spatial distribution and time span of this OIB-like basaltic magmatism are better explained by a model involving the development of a tear in the downgoing Nazca slab. This tear evolved into a unique slab window parallel to the trench, by the combined processes of plate detachment (sinking of the deep part of the Nazca plate) and thermal erosion of the slab window edges (Thorkelson and Breitsprecher, 2005), during the first Chile Ridge-trench collision events at ca. 15–12 Ma. Petrogenetic studies of the Pliocene to Quaternary MLBA post-plateau mafic lavas indicate that they were generated from an asthenospheric source and then ascended through a completely opened slab window under the Lago General Carrera–Buenos Aires region (Gorring et al., 2003).

Several bodies of felsic rocks intruding early Pliocene volcanic sequences, associated with scarce lava flows, are exposed on the western side of the MLBA (Fig. 2) and have been recently mapped by Giacosa and Franchi (2001). These felsic rocks are volumetrically minor when compared with the contemporaneous MLBA mafic rocks, and are unknown elsewhere in the NPPL. However, the occurrence of 5–7 Ma old peralkaline rhyolite obsidian archeological artifacts has been reported by Stern (1999, 2004), and that of ca. 9 Ma old fluidal rhyolitic flows in the Meseta Chile Chico by Espinoza et al. (2005a). In the MLBA, a complete felsic sub-volcanic system coeval with basaltic volcanism is exposed, which represents a unique opportunity to study their genetic relationships.

The aim of this study is to investigate the chronological, petrological, geochemical and isotopic characteristics of these felsic alkaline rocks and to evaluate their genetic relationship with the coeval and younger MLBA basalts. Our results allow us to propose a petrogenetic model of this bimodal felsic–mafic magmatism and to relate it with the Neogene plate dynamics in Patagonia.

2. Tectonic setting and regional geology

The Meseta del Lago Buenos Aires (MLBA) basaltic plateau is located south of the Lake General Carrera–Buenos Aires (LGCBA), ~320 km southeast of the present

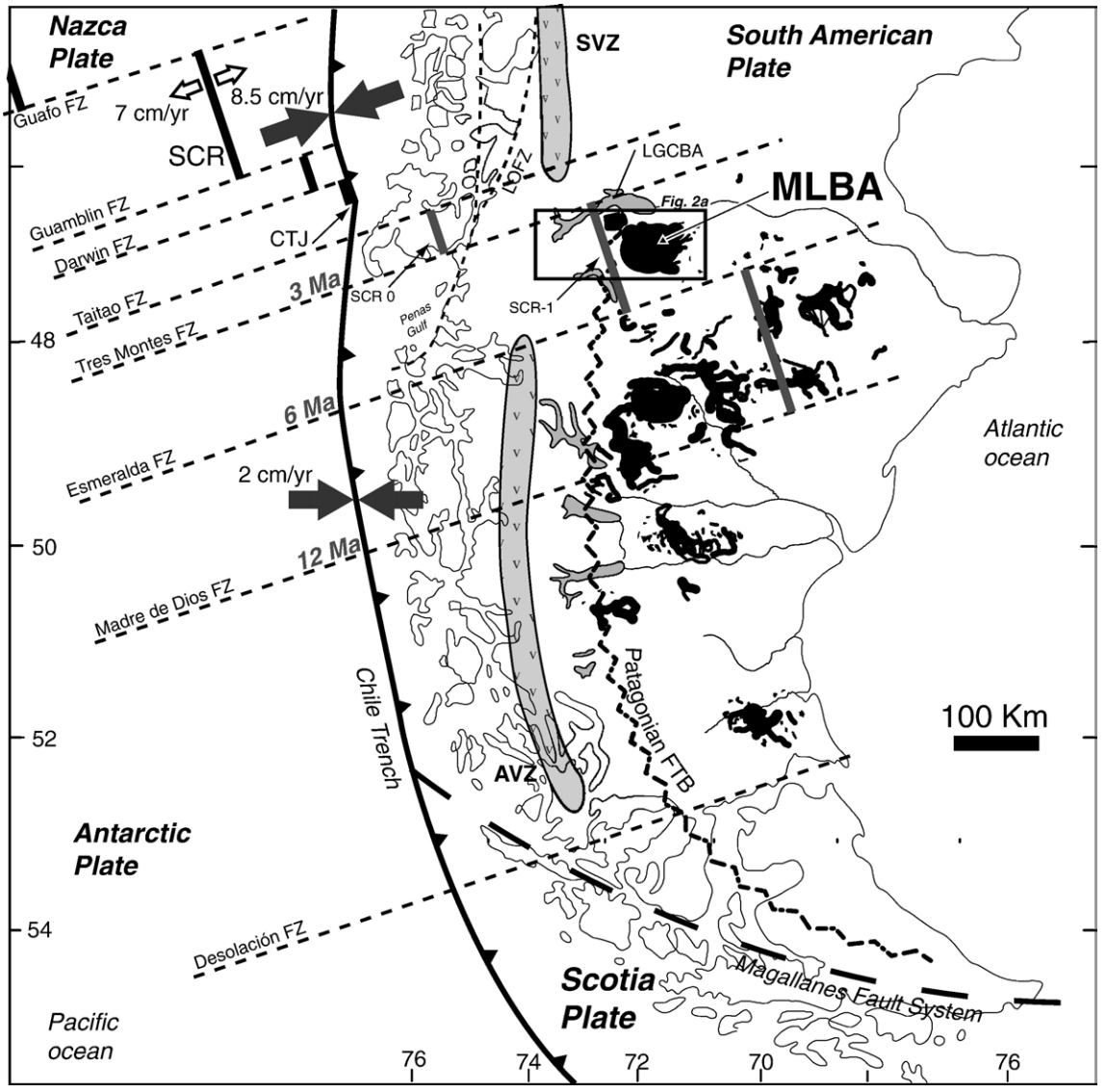

Fig. 1. Present day tectonic setting of Southern South America showing lithospheric plates configuration, oceanic Fracture Zones (FZ), South Chile Ridge (SCR) segments, Chile Triple Junction (CTJ) (after Cande and Leslie, 1986) and the location of the Meseta del Lago Buenos Aires (MLBA) in the context of the Neogene Patagonian Plateau Lavas (in black, after Gorring et al., 1997). Dark grey arrows indicate the relative plate motion of the Nazca and Antarctic Plate with respect to the South American Plate; numbers are relative velocities in cm/yr (after DeMets et al., 1990). Expected positions of subducted segments of the Chile Ridge (SCR0 to SCR-2) below southern South America are represented as thick grey lines. Gray numbers (in Ma) indicate the time of collision of the different segments of the Chile Ridge with the Chile Trench. LGCBA: Lago General Carrera–Buenos Aires; SVZ, AVZ: Southern and Austral Volcanic Zones of the Andes; PFTB: Patagonian Fault and Thrust Belt; LOFZ: Liquiñe–Ofqui Fault Zone.

location of the Chile Triple Junction generated between the subducting Antarctic and Nazca oceanic plates and the South American continent (45°46′S), and ca. 150 km east of the volcanic arc gap between the Southern and Austral Volcanic Zones of the Andes (Fig. 1).

To the west of the study area, the Cordillera is constructed by overthrusted blocks and folded sequences of the Early Jurassic–Early Cretaceous Ibáñez Group (part of the Mesozoic Chon-Aike acid Large Igneous Province; Pankhurst et al., 1998), made up of felsic volcanics and tuffs together with continental sedimentary deposits. These rocks overlie unconformably the Eastern Andean Metamorphic Complex, an Early Carboniferous greenschist sequence of metasedimentary and meta-volcanic rocks (Ramos, 1989; Hervé et al., 1998; Bell and Suárez, 2000). The tectonic front of the Cordillera in the LGCBA region consists of four en échelon segments of these Late Paleozoic–Mesozoic

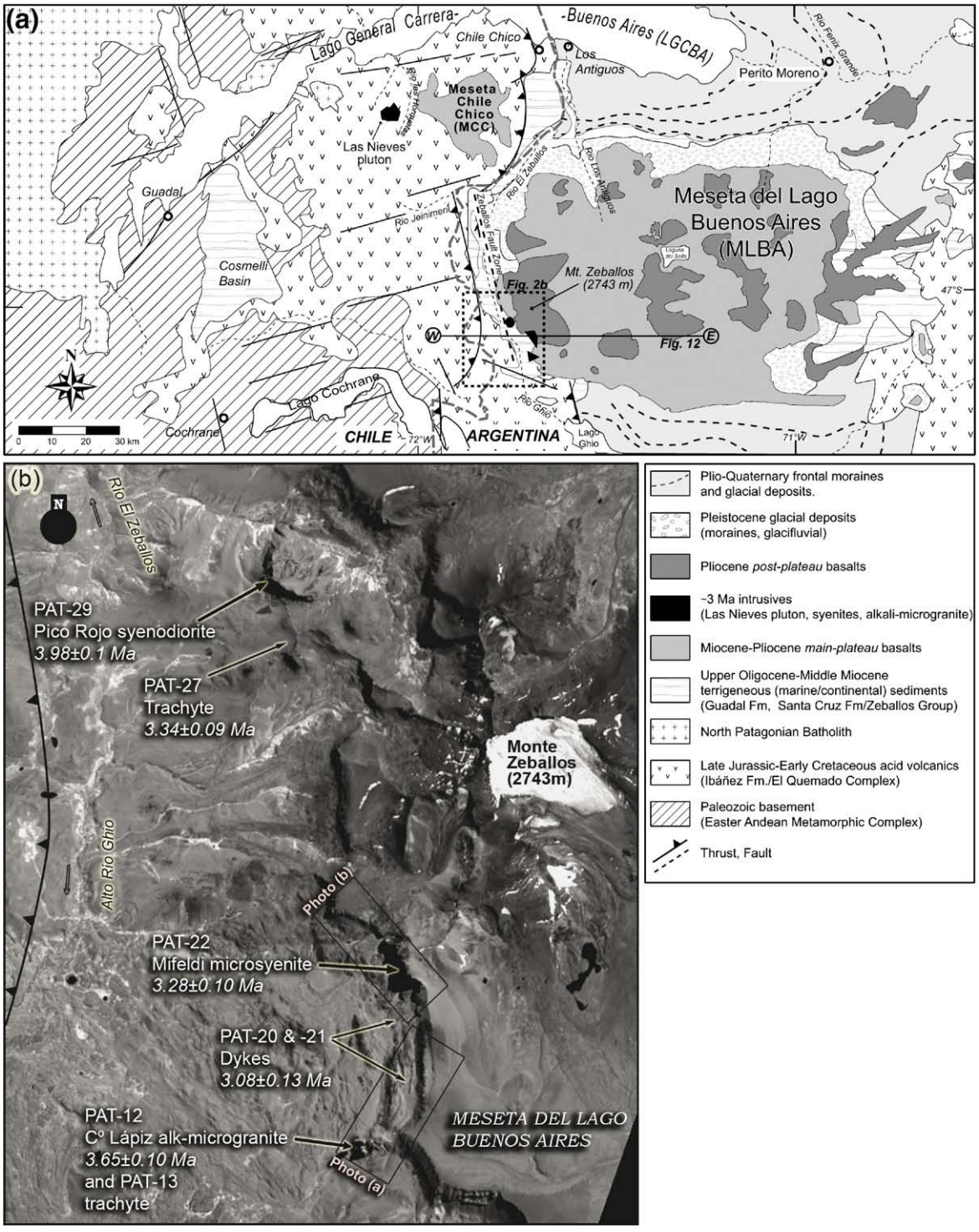

Fig. 2. a) Geological map of the area south of Lago General Carrera–Buenos Aires (modified from Lagabrielle et al., 2004), location of the study area is shown by a frame; b) SPOT satellite image of the southwestern flank of the MLBA (Zeballos Fault Zone area) east of the morphotectonic front of the Cordillera, showing the location and the ages (Ma± 1σ) of studied intrusions and lava flows. Field photographs a) and b) in Fig. 3.

rocks, separated by fault zones with dominant N160–N170 strike-slip displacement (Lagabrielle et al., 2004). Further west, sub-parallel to the present coastline, outcrops the Patagonian Batholith, a continuous body about 1000 km long and 200 km wide consisting of Late Jurassic to Pliocene subduction-related intrusive rocks (Weaver et al., 1990; Bruce et al., 1991; Hervé et al., 2000, 2007).

The up to 300 m-thick basal lava sequence of the MLBA overlies unconformably the synorogenic sediments of the Río Zeballos Group (late Early to early Middle Miocene; Ugarte, 1956; Marshall and Salinas, 1990; Flint et al., 1994; Escosteguy et al., 2002) and locally the Jurassic volcanics. This ca. 1500 km^3 main-plateau basaltic pile (which determines the overall plateau-like morphology of the meseta) comprises tabular basaltic lava flows and necks (Hashimoto et al., 1977; Busteros and Lapido, 1983; Giacosa and Franchi, 2001) emplaced during Upper Miocene–Lower Pliocene (~12.2–3.3 Ma, Guivel et al., 2006) (Fig. 2a). Later, post-plateau MLBA basalts (Gorring et al., 2003; Fig. 2a) were emplaced in several volcanic pulses during the last 3.4 Ma–100 ka (Baker et al., 1981; Ton-That et al., 1999; Brown et al., 2004; Singer et al., 2004) as monogenetic cones, maars and fluid flows filling incisions and valleys dug into the main-plateau sequence (Guivel et al., 2006). They are volumetrically minor (~600 km^3, Gorring et al., 2003) compared to the main sequence. In the southwestern border of the MLBA, close to the Monte Zeballos area (Fig. 2b), several felsic sub-volcanic bodies (shallow level plugs and dykes) crosscutting Early Pliocene basalts and related evolved lavas outcrop at altitudes around 1800–2000 m a.s.l. These rocks have been described by Giacosa and Franchi (2001) as the Cerro Lápiz trachyte volcanic suite, mainly composed by sub-volcanic bodies, disrupted volcanoes and eroded short lava flows. Previous $^{40}Ar/^{39}Ar$ dates reported by Brown et al. (2004) for some of these felsic intrusions indicate ages around 3.2 Ma. In addition, the Las Nieves pluton, a small and isolated 3.2±0.4 Ma old meta-aluminous biotite quartz-monzonite (Morata et al., 2002), is located within a fold and thrust zone intruding the Jurassic volcanic sequence (Fig. 2a) 55 km northwest of the studied area (46°40′S).

3. Field observations

The studied felsic rocks correspond to three plugs, two dykes and two lava flows sampled on the western flank of MLBA exposed along the Alto Ghio–El Zeballos rivers glacial valley (Fig. 2b). This valley corresponds to a N160–170 tectonic corridor (Zeballos Fault Zone; Lagabrielle et al., 2004, submitted for publication) defined here by the morphotectonic front of one segment of the Patagonian Cordillera to the west and by the vertical scarp of MLBA to the east (Fig. 2). The number of samples collected was limited due to difficult access conditions, but they are thought representative of the main morphological and geological units exposed in the studied area (Figs. 2b and 3). All the studied rocks were fresh enough for geochemical analysis (Loss On Ignition values lower than 1.5 wt.%) and whole-rock K–Ar dating (Table 1).

The studied rocks from south to north are discussed in the following subsections.

3.1. Cerro Lápiz microgranite

It is a pencil-shaped neck intruding Mio-Pliocene basalts connected to the MLBA plateau only by a slumped basaltic pile and intercalated sediments cooked by the intrusion (Fig. 3a). An associated trachytic vesicular lava flow was sampled very close to the intrusive.

3.2. Mifeldi microsyenite

Located 4 km north from Cerro Lápiz, it is a lenticular-shaped intrusion forming a ~200 m high N–S trending vertical scarp which coincides here with the

Table 1
Whole-rock K–Ar ages of Pliocene western Meseta del Lago Buenos Aires felsic rocks and Las Nieves granite

Unit–sample		Structure	Rock type	Location	^{40}Ar–^{39}Ar ages (Ma±2σ) (Brown et al., 2004)	Fused weight of sample (g)	$^{40}Ar^*$ ($\times10^{-7}$ cm^3/g)	$^{40}Ar^*$ (%)	Age (Ma)	±	Error (1σ)
Cerro Lápiz	PAT-12	Neck	Alkali granite	SW-MLBA	3.18±0.04	0.806	5.74	48.2	3.65	±	0.10
Mifeldi	PAT-20	Dyke	Microsyenite	SW-MLBA		0.803	4.61	23.9	3.08	±	0.13
	PAT-22	Laccolith	Microsyenite	SW-MLBA	3.29±0.22	0.8093	4.49	34.8	3.28	±	0.10
Pico Rojo	PAT-27	Lava	Trachyte	W-MLBA		0.4325	4.49	44.9	3.34	±	0.09
	PAT-29	Neck	Syeno-diorite	W-MLBA		0.4583	3.94	66.6	3.98	±	0.1
Las Nieves	CC-138*	Pluton	Granite	Las Nieves river					3.20	±	0.40

Decay constants: $\lambda e = 0.581\times10^{-10}$ yr^{-1}; $\lambda_\beta = 4.96\times10^{-10}$ yr^{-1}; $^{40}K/K_{total} = 0.0167$.
*Analyzed at SERNAGEOMIN, Chile (Morata et al., 2002).

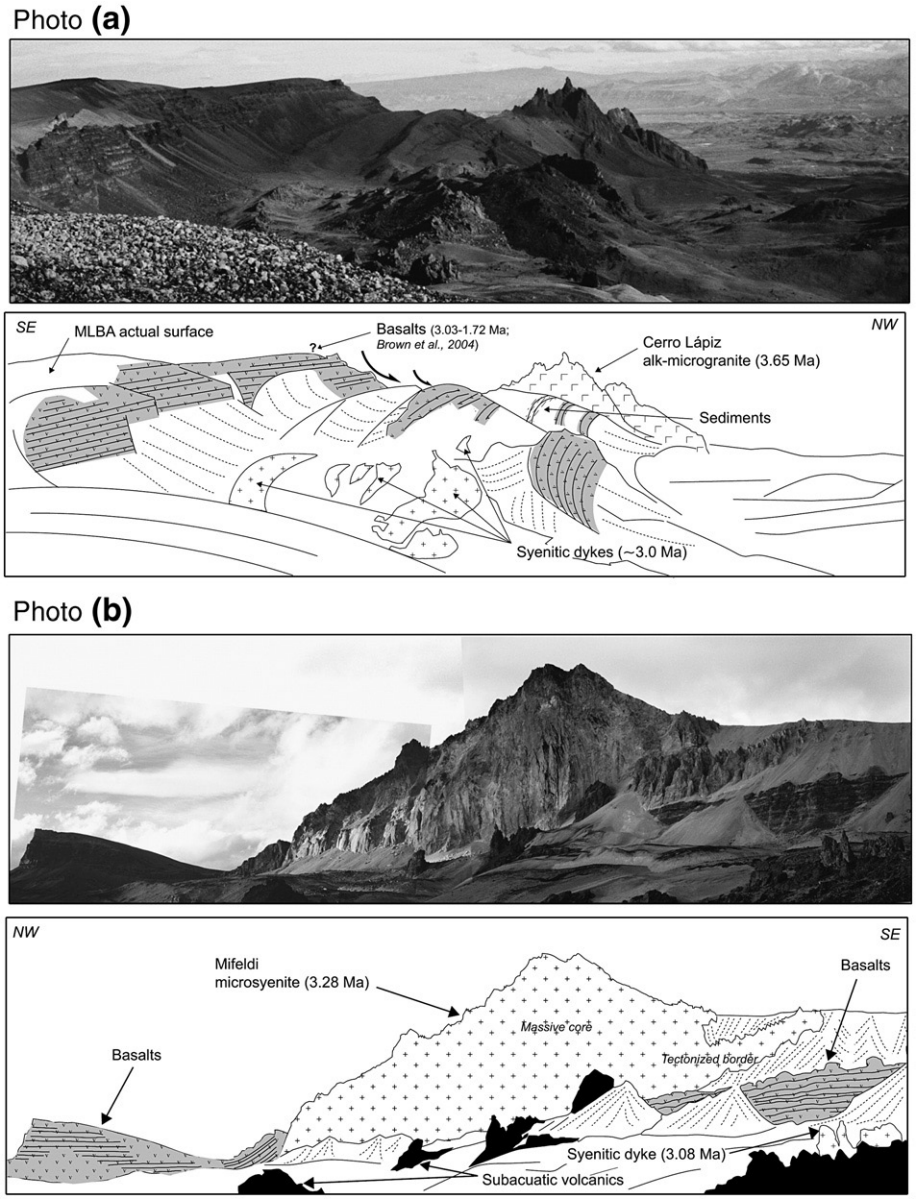

Fig. 3. Field photographs and corresponding graphic sketches of (a) Cerro Lápiz alkali microgranite and (b) Mifeldi microsyenite. Note in (a) the disposition of N160–170 syenitic dykes along inferred normal faults delimitating slump sliding, and in (b) the intrusive relationships (laccolith-like) between the microsyenite and the basaltic flows. Note also in b) the contrasted textures of the massive core and the tectonized border of the intrusion, and the occurrence of a N160E dyke. (?): inferred location. See location of photographs in Fig. 2b.

MLBA border. Clear crosscutting and horizontal (laccolith-like) intrusive relationships with Mio-Pliocene basalts are visible along the nice exposure of this longitudinal section (Fig. 3b). Close to the outcrop, numerous blocks of syenite including felsic xenoliths were found. In addition, several ~N160–170 trending sub-vertical syenitic dykes occur immediately south of the major intrusion, within a shallow depression that runs south towards the Cerro Lápiz neck (Fig. 3a and b).

3.3. Pico Rojo syeno-diorite

This huge sub-circular neck is rimmed to the east by a glacial valley which erases any contact with the MLBA basalts. It is located 9 km north from Mifeldi microsyenite in a region where numerous basaltic dykes and necks crosscutting the Miocene sediments are exposed, which could represent the feeders of the Mio-Pliocene MLBA volcanism (no field relationships were observed between

Table 2
Representative EMPA mineral chemistry analysis of western Meseta del Lago Buenos Aires felsic rocks

Mineral	Feldspars								Pyroxenes								
Sample	PAT-12	PAT-12	PAT-12	PAT-13	PAT-13	PAT-20	PAT-20	PAT-20	PAT-20	PAT-20	PAT-20	PAT-20	PAT-29	PAT-29	PAT-13	PAT-13	PAT-13
Unit	C. Lápiz	C. Lápiz	C. Lápiz	C. Lápiz	C. Lápiz	Mifeldi	Mifeldi	Mifeldi	Mifeldi	Mifeldi	Mifeldi	Mifeldi	Pico Rojo	Pico Rojo	C. Lápiz	C. Lápiz	C. Lápiz
Rock	Alk-Gr	Alk-Gr	Alk-Gr	Trachyte	Trachyte	m-syenite	m-syenite	m-syenite	m-syenite	m-syenite	m-syenite	m-syenite	sy-diorite	sy-diorite	Trachyte	Trachyte	Trachyte
Observation	Core	Rim	GM	Core	Rim	Core	Rim	GM	Core	Rim	GM	Core	Core	Core	Core	Rim	GM
SiO_2	65.05	64.93	65.55	66.07	66.26	59.11	65.56	66.02	49.80	50.02	51.68	55.46	48.94	49.10	51.51	47.86	47.35
TiO_2	0.00	0.00	0.01	0.07	0.00	0.00	0.07	0.20	1.16	0.17	0.28	0.01	0.24	1.35	0.07	0.00	0.27
Al_2O_3	19.31	20.07	20.71	19.36	19.39	24.83	20.62	18.44	3.28	0.77	0.23	0.02	0.14	3.58	0.46	0.96	0.84
FeO	0.28	0.38	0.22	0.14	0.32	0.32	0.41	0.47	10.92	19.55	28.10	14.03	34.17	10.80	16.95	27.09	28.76
MnO	0.00	0.00	0.00	0.01	0.07	0.00	0.07	0.00	0.41	0.71	1.02	1.90	1.63	0.35	0.62	1.33	1.32
MgO	0.00	0.00	0.03	0.00	0.02	0.03	0.01	0.00	14.21	8.32	13.34	28.62	10.97	13.57	9.15	2.62	1.63
CaO	0.51	1.45	2.51	0.74	1.21	6.91	2.14	0.25	18.98	19.14	4.46	0.20	3.07	20.60	20.94	19.21	19.26
Na_2O	4.98	6.91	8.37	5.49	6.83	7.40	9.05	5.25	0.57	0.46	0.08	0.00	0.11	0.47	0.45	0.29	0.32
K_2O	9.41	5.72	2.29	8.42	6.63	0.57	2.13	9.49	0.00	0.02	0.00	0.01	0.00	0.03	0.00	0.00	0.00
Total	99.54	99.47	99.70	100.29	100.72	99.18	100.06	100.11	99.33	99.16	99.20	100.31	99.27	99.85	100.16	99.35	99.74
Si	2.959	2.925	2.910	2.968	2.956	2.666	2.905	2.988	1.868	1.965	2.000	1.985	1.975	1.837	1.985	1.957	1.945
Ti	0.000	0.000	0.000	0.002	0.000	0.000	0.002	0.007	0.033	0.005	0.008	0.000	0.007	0.038	0.002	0.000	0.008
Al	1.035	1.066	1.083	1.025	1.019	1.320	1.077	0.983	0.145	0.035	0.011	0.001	0.007	0.158	0.021	0.046	0.041
Fe^{2+}	0.011	0.014	0.008	0.005	0.012	0.012	0.015	0.018	0.250	0.584	0.920	0.393	1.120	0.213	0.511	0.869	0.915
Fe^{3+}									0.095	0.061	0.000	0.028	0.037	0.128	0.037	0.062	0.079
Mn^{2+}	0.000	0.000	0.000	0.000	0.003	0.000	0.003	0.000	0.013	0.024	0.034	0.058	0.056	0.011	0.020	0.046	0.046
Mg	0.000	0.000	0.002	0.000	0.001	0.002	0.000	0.000	0.794	0.487	0.778	1.527	0.660	0.757	0.526	0.160	0.100
Ca	0.025	0.070	0.120	0.035	0.058	0.334	0.102	0.012	0.763	0.806	0.187	0.008	0.133	0.826	0.865	0.842	0.848
Na	0.439	0.603	0.721	0.478	0.591	0.647	0.777	0.461	0.042	0.035	0.006	0.000	0.009	0.034	0.034	0.023	0.026
K	0.546	0.329	0.130	0.483	0.377	0.033	0.121	0.548	0.000	0.001	0.000	0.000	0.000	0.001	0.000	0.000	0.000
Sum	5.016	5.008	4.973	4.997	5.018	5.014	5.003	5.017	4.003	4.003	3.944	4.001	4.004	4.004	4.002	4.005	4.007

Cation per formula unit of representative plagioclase based on 8O and pyroxenes on 6O.
Alk-Gr: alkali granite; m-syenite: microsyenite; sy-diorite: syeno-dirite.
GM: groundmass.

Table 3
Representative ICP-MS and ICP-AES geochemical analyses of Pliocene western Meseta del Lago Buenos Aires felsic rocks and Las Nieves granite

Sample no.	PAT-12	PAT-13	PAT-20	PAT-21	PAT-22	PAT-27	PAT-29	CC-138**
Age [Ma]	3.65	–	3.08	–	3.28	3.34	3.98	3.2
UTM E	292340	292340	292728	293428	293488	290427	290092	723419
UTM S	4778705	4778705	4780366	4780915	4781845	4789707	4790381	4825965
Unit	C. Lápiz	C. Lápiz	Mifeldi	Dyke	Mifeldi	Pico Rojo	Pico Rojo	Las Nieves
Rock type	Alkali granite	Trachyte	Microsyenite	Microsyenite	Microsyenite	Trachyte	Syeno-diorite	Quartz-monzonite
Major elements								
SiO_2	68.1	65.2	65	62.8	63.6	60.9	59.6	63.7
TiO_2	0.12	0.23	0.66	0.78	0.67	0.6	1.24	0.85
Al_2O_3	15.5	16.05	15.8	16.4	16.5	16.55	15.3	16
$Fe_2O_{3\_total}$	3.16	5.14	5.44	6	5.65	7.13	7.9	4.88
MnO	0.01	0.14	0.11	0.12	0.1	0.27	0.18	0.09
MgO	0.09	0.1	0.79	1.09	0.91	0.62	1.52	1.72
CaO	0.74	1.7	2.22	2.75	2.44	2.4	3.8	3.29
Na_2O	5.32	5.14	5.12	5.22	5.28	5.86	5.18	4.34
K_2O	5.35	5.66	4.64	4.3	4.44	4.68	3.51	3.81
P_2O_5	0.03	0.07	0.28	0.38	0.3	0.29	0.61	0.23
L.O.I.	1.52	0.48	0.09	0.04	0.23	0.74	1.48	1
TOTAL	99.94	99.91	100.15	99.88	100.12	100.04	100.32	99.63
Trace elements (ppm)								
Rb	122	96.8	136	115	120.5	91.1	82.3	
Sr	16.4	81	237	319	299	259	356	400
Ba	206	1185	790	874	869	1489	867	590
Sc*	1.5	8.5	7.5	8.7	8	16	15.5	10
V*	2	2	19	29	24	3	47	75
Cr*	3	3	3	3	3.5	1.5	2.5	5
Co*	0	0	5	6.5	5	2.5	7.5	11
Ni*	1	1	1.5	2	1.5	1	1	5
Y	41.3	49.5	36	31.1	30.4	41.8	39.8	26
Zr*	250	116	59	107	43	550	273	395
Nb	94.7	77.3	56	51.9	52.2	56.3	42.4	21
Cu	4.7	4.91		6.1	4.48	4.26	6.55	18
Zn	116	147		104.3	111.6	125	116	79
Ga	29.6	28		26.3	27.3	26.2	24.7	
Ge	2.17	2.09		161	1.69	1.782	1.72	
As	3.05	2.41		210	2.46	1.029	1.38	
Mo	6.35	4.77		376	4.69	3.95	3.1	
Cd	0.041	0.164		0.098	0.128	0.1222	0.1331	
Sn	3.79	2.39		240	2.98	2.05	2.68	
Cs	1.78	1.36		324	3.75	1.39	1.576	
La	164	179	74	66.7	68.6	70.95	48.4	43
Ce	288	325	137	135.4	137.7	145.5	105.7	97
Pr	30.6	32.4		13.6	13.51	14.99	11.42	
Nd	106	115	48	48.9	47.8	55.4	45.3	44
Sm	17.3	18.2	8.5	8.6	8.3	10.14	9.27	7.24
Eu	1.46	2.89	1.8	2.12	1.92	3.16	2.76	1.36
Gd	11.6	12.7	7.2	6.78	6.51	8.17	8.16	5.29
Tb	1.69	1.84		1.023	1.009	1.26	1.257	
Dy	9.13	10.2	6.2	5.93	5.93	7.54	7.4	5.35
Ho	1.63	1.96		1.161	1.122	1.538	1.476	1.11
Er	4.07	5.43	3.1	3.19	3.11	4.4	4.16	3.02
Tm	0.518	0.759		0.438	0.437	0.646	0.586	
Yb	3.08	4.73	3	2.77	2.71	4.18	3.67	2.98
Lu	0.419	0.731		0.408	0.393	0.658	0.559	0.44
Hf	6.8	3.4		2.74	1.022	12.41	6.73	9
Ta	5.17	4.1		3.34	3.37	3.19	2.5	

Table 3 (*continued*)

Sample no.	PAT-12	PAT-13	PAT-20	PAT-21	PAT-22	PAT-27	PAT-29	CC-138**
Age [Ma]	3.65	–	3.08	–	3.28	3.34	3.98	3.2
UTM E	292340	292340	292728	293428	293488	290427	290092	723419
UTM S	4778705	4778705	4780366	4780915	4781845	4789707	4790381	4825965
Unit	C. Lápiz	C. Lápiz	Mifeldi	Dyke	Mifeldi	Pico Rojo	Pico Rojo	Las Nieves
Rock type	Alkali granite	Trachyte	Microsyenite	Microsyenite	Microsyenite	Trachyte	Syeno-diorite	Quartz-monzonite
Trace elements (ppm)								
Pb	14.77	12.96		11.48	26.45	8.23	10.23	
Tl	0.166	0.244		0.164	0.686	0.1173	0.288	
Th	17.8	14.7	18	14.7	15.35	10.67	8.83	19
U	1.9	1.86		3.37	2.39	2.38	2.16	

** Las Nieves granite analyzed by ICP-AES at Sernageomin, Chile (Morata et al., 2002).
PAT-20 and marked (*) elements measured by ICP-AES. Relative standard deviation is ca. 1% for SiO_2 and 2% for the other major elements except for low values (<0.50% oxide) for which the absolute standard deviation is 0.01%. For minor elements, relative standard deviation is ca. 5% except for concentrations below six times the detection limit, for which the absolute standard deviation is about one third of the detection limit. Detection limits are 2 ppm for Ba, V, Cr, Co, Ni, Zr and Ce; 1 ppm for Nd, Gd and Er; 0.5 ppm for Rb, Sr, Nb, La and Sm; 0.3 ppm for Y, Dy and Th; 0.15 ppm for Sc, Eu and Yb.

them and the felsic intrusives). This rock contains decimetric felsic xenoliths. A trachytic lava flow occurring near this neck, at 2000 m a.s.l., has also been sampled.

4. Analytical methods

Whole-rock ^{40}K–^{40}Ar ages were obtained at the geochronology laboratory of the Université de Bretagne Occidentale (Brest, France). Analyses were performed on the 0.5- to 0.15-mm-size fraction after crushing, sieving and cleaning with distilled water of whole-rock samples. One aliquot of sample was powdered for K analysis by atomic absorption after HF chemical dissolution and 0.5–0.15-mm grains were used for argon isotopic analyses. Argon extraction was performed by the direct technique under high vacuum (10^{-5}–10^{-7} hPa) using induction heating of a molybdenum crucible. The argon content was measured by isotope dilution and argon isotopes were analyzed in an 1808-geometry stainless steel mass spectrometer, according to the original procedure described by Bellon et al. (1981). Age calculations, following the equation of Mahood and Drake (1982) and using the Steiger and Jäger's (1977) recommended constants, are given, with 1σ error, in Table 1.

Mineral chemistry (Table 2) was carried out at Microsonde Ouest (Brest, France), using a five spectrometer Probe CAMEBAX SX-50. Analytical conditions were 15 nA, 15 kV, counting time 6 s, using natural standards as reference and ZAF corrections. A detailed account of the procedure is given in Defant et al. (1991).

Major and selected trace element analyses (Table 3) were performed on agate-ground powders by ICP-AES at the chemical laboratory of the Université de Bretagne Occidentale (Brest, France). All data were calculated using IWG-GIT, BE-N, AC-E, PM-S and WS-E as standards. Specific details for the analytical methods and sample preparation can be found in Cotten et al. (1995).

Trace element analyses (Table 3) were performed by ICP-MS using an Elan 6000 Perkin Elmer quadripolar ICP-MS at the LMTG (Toulouse, France). Calibrations, internal standard and interferences corrections were done following the procedure described in Aries et al. (2000).

Table 4
Sr–Nd isotopic data for Pliocene western Meseta del Lago Buenos Aires felsic rocks

Sample	Rock type	Age (Ma±1σ)	Rb (ppm)	Sr	Sm	Nd	$^{87}Rb/^{86}Sr$	$^{87}Sr/^{86}Sr$	$(^{87}Sr/^{86}Sr)_o$	$^{147}Sm/^{144}Nd$	$^{143}Nd/^{144}Nd$	$(^{143}Nd/^{144}Nd)_o$	eNd_{CHUR}
PAT-12	Syenite	3.65±0.1	122.4	16.4	17.32	106.12	21.5589	0.70682	0.70570	0.0987	0.51261	0.512608	−0.5
PAT-13	Trachyte	–	96.8	81.0	18.21	115.03	3.4564	0.70574	0.70556	0.0957	0.512605	0.512603	−0.6
PAT-21	Syenite (dyke)	3.08±0.13	115.0	319.0	8.60	48.92	1.0428	0.70493	0.70488	0.1064	0.512647	0.512645	0.2
PAT-22	Syenite	3.28±0.10	120.5	299.2	8.30	47.78	1.1651	0.70499	0.70494	0.1050	0.512637	0.512635	0.0
PAT-27	Trachyte	3.34±0.09	91.1	259.1	10.14	55.43	1.0172	0.70505	0.70501	0.1107	0.512635	0.512633	0.0
PAT-29	Syeno-diorite	3.98±0.1	82.3	356.3	9.27	45.27	0.6681	0.70573	0.70571	0.1239	0.512647	0.512645	0.2

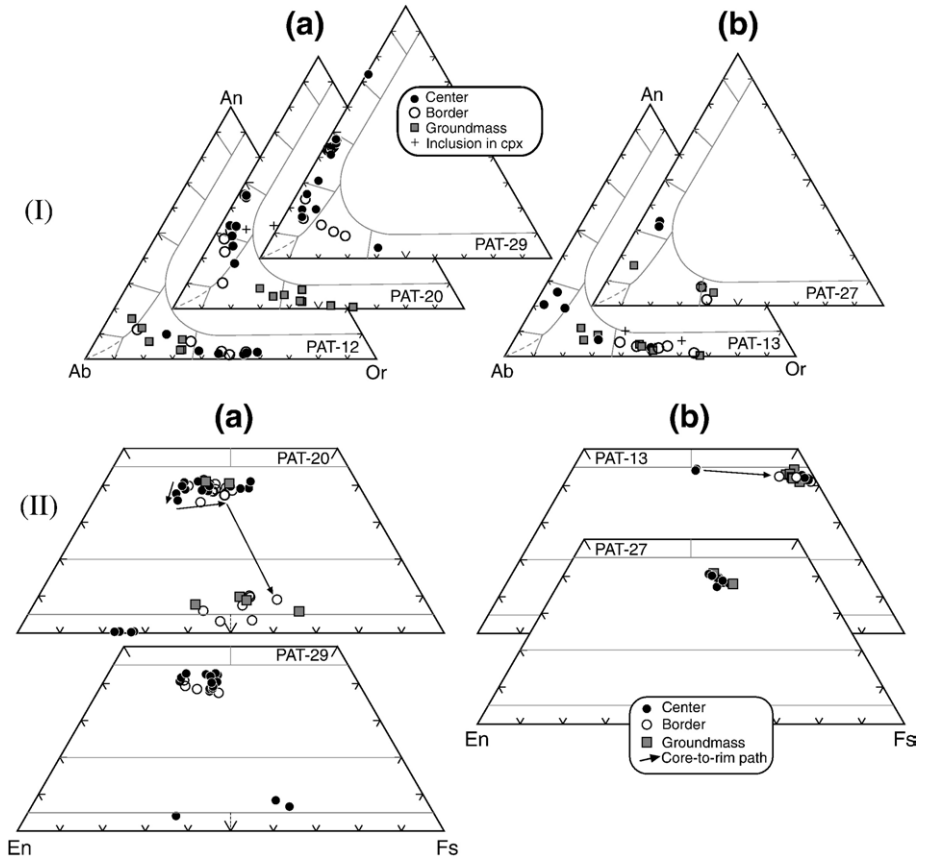

Fig. 4. I) Ab–An–Or compositional triangles for feldspar phenocrysts and groundmass of W-MLBA felsic rocks. II) Classification diagrams for pyroxene phenocrysts and groundmass of W-MLBA felsic rocks (Morimoto et al., 1988); a) intrusive rocks, b) lava flows.

Data quality was controlled by running BCR-2 standard. Relative standard deviations are generally ≤5%.

The Sr and Nd isotopic compositions of six selected samples (Table 4) were analyzed on a Finnigan-Mat 261 multicollector mass spectrometer at the LMTG (Toulouse, France). Sr and Nd were first separated from the matrix using the Sr SPEC, LN-SPEC and TRU-SPEC resins, following the technique set up by Pin et al. (1995). Sr was loaded on a W single filament with a TaCl 'activator' and Nd was loaded on one of two Re filaments. The La Jolla standard was run regularly and isotopic ratios were corrected for any laboratory bias, as described in Benoit et al. (1996).

5. Geochronology

The three intrusives, the dyke and two lava flows, display K–Ar ages between 3.98 and 3.08 Ma (Table 1), roughly synchronous with the beginning of the post-plateau basaltic magmatism in the MLBA (3.4–3.3 Ma, Baker et al., 1981; Ton-That et al., 1999; Brown et al., 2004) and with the basal lava flow of a basaltic pile located close to the Cerro Lápiz neck (3.03±0.3 Ma; Brown et al., 2004; Fig. 3a). These ages closely match those obtained with the ^{40}Ar–^{39}Ar method by Brown et al. (2004) for two of the same rocks (see Table 1). This felsic magmatism is also coeval with the 3.2±0.4 Ma old Las Nieves pluton (Morata et al., 2002), exposed 55 km northwest (Fig. 2a).

6. Petrography and mineral chemistry

6.1. Intrusives

In the Cerro Lápiz neck (sample PAT-12), alkali feldspar (up to 50 % in volume) showing sanidine K-rich cores ($An_3Ab_{43}Or_{54}$) and anorthoclase rims ($An_7Ab_{60}Or_{33}$) is the only microphenocryst, set in a fine-grained trachytic groundmass of Na-rich plagioclase laths ($An_{4-16}Ab_{63-76}Or_{8-31}$) and Fe–Ti oxides (Fig. 4Ia). Besides, several tiny (<20 μm) interstitial late stage mineral phases were recognized through SEM–EDS qualitative analyses. Among them, monazite, allanite, Ce-aeschynite ((Ce,Ca,

Fe)(Ti,Nb)$_2$(O,OH)$_6$), thorite ($ThSiO_4$), thorianite (ThO_2), and baddeleyite (ZrO_2) are the most abundant, and show high contents of trace elements like Th, U, Zr, Nb, Y and light rare earth (La, Ce, Nd) elements (Fig. 5a).

Mifeldi intrusive and dykes (samples PAT-20, -21 and -22) show a porphyritic texture; highly zoned plagioclase (25 modal %; $An_{45-10}Ab_{52-77}Or_{2-12}$) dominates over zoned augitic clinopyroxenes (5 modal %; $Wo_{41-40}En_{40-35}Fs_{19-25}$). Pigeonite ($Wo_{3-10}En_{30-57}Fs_{30-63}$) forms the external rims of some clinopyroxene phenocrysts and also occurs as disseminated grains in the groundmass (Fig. 4IIa). Rare orthopyroxenes ($En_{76-72}Fs_{24-28}$), amphibole pseudomorphs (completely replaced by biotite + Fe–Ti oxides), minor Fe–Ti oxides and accessory apatite and zircon can be found in a fine-grained trachytic groundmass mostly made up of anorthoclase and sanidine ($An_{1-8}Ab_{45-66}O_{54-26}$; Fig. 4Ia).

Pico Rojo neck (sample PAT-29) is an inequigranular holocrystalline rock with strongly zoned plagioclase (55 modal %) ($An_{16-73}Ab_{77-26}Or_{7-1}$) and anorthoclase ($An_{13-4}Ab_{72-57}Or_{15-39}$; Fig. 4Ia), clinopyroxene (10 modal %, $Wo_{41-38}En_{42-37}Fs_{18-22}$) and unaltered Fe–Ti oxide (3 modal %) phenocrysts. Rare pigeonite ($Wo_{4-8}En_{32-60}Fs_{35-60}$) forms the core of some microphenocrysts (Fig. 4IIa). Characteristically this sample contains quartz xenocrysts with a clinopyroxene reaction rim compositionally similar to the phenocrysts ($Wo_{37-40}En_{24-40}Fs_{22-37}$). Accessory apatite and zircon are also present.

6.2. Lava flows

Close to the Cerro Lápiz neck, a vesicular trachytic lava (PAT-13) is made up of phenocrysts of normally- and reversely-zoned potassic oligoclase (5 modal %)

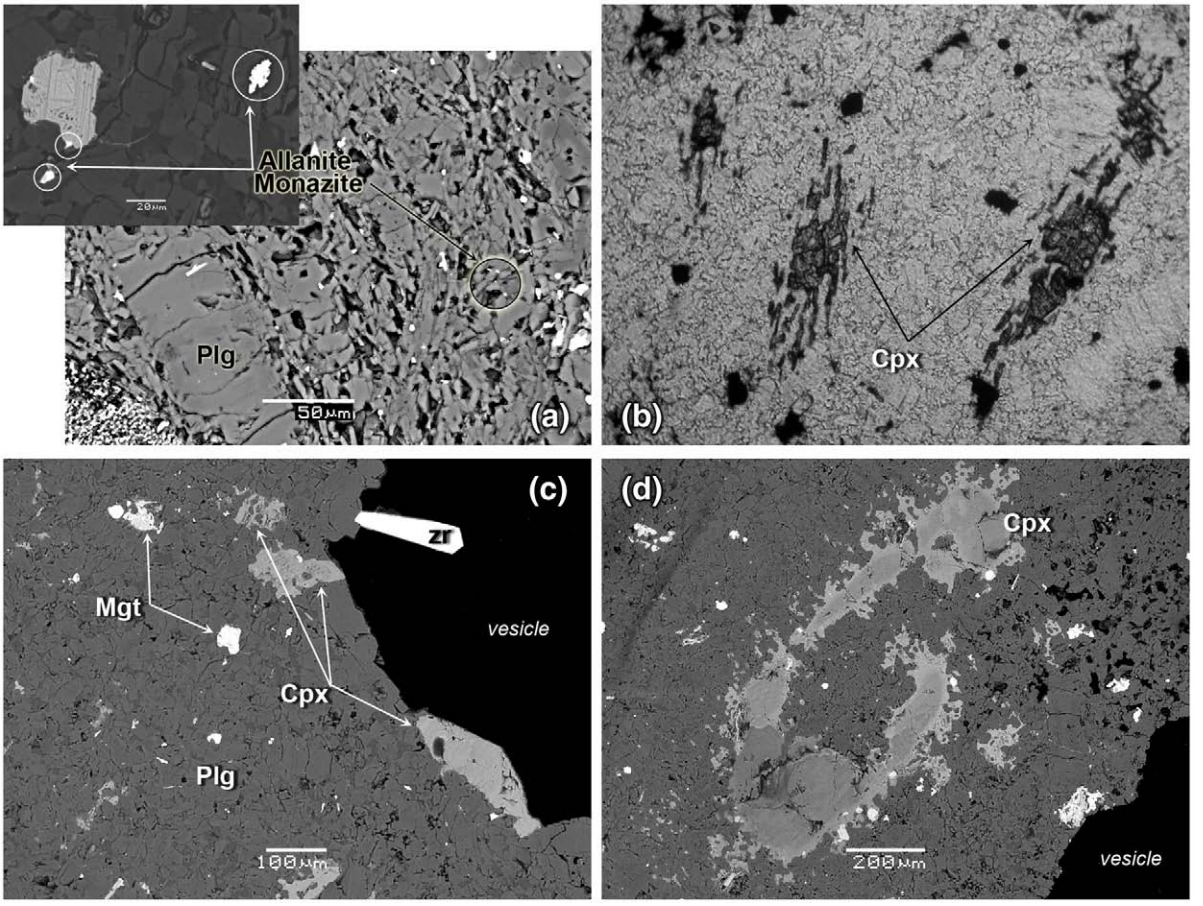

Fig. 5. a) SEM images showing the occurrence of tiny interstitial incompatible trace elements-rich mineral phases (allanite, monazite, among others) in sample PAT-12 alkali microgranite; b) microphotograph (100×, non-polarized light) of the groundmass of PAT-13 trachyte, note the interstitial growths of green ferro-hedenbergite between feldspars; c) SEM image of a vesicle in sample PAT-13 with grown euhedral crystals of ferro-hedenbergite and zircon, note the different textures of clinopyroxene in the groundmass; d) SEM image of a zoned subhedral primary clinopyroxene with an augitic core and ferro-hedenbergitic rim in PAT-13 trachyte (see compositional trend for this pyroxene in Fig. 4IIb).

($An_{19-26}Ab_{70-69}Or_{11-5}$) and anorthoclase–sanidine ($An_{2-7}Ab_{34-64}Or_{64-29}$; Fig. 4Ib), set in a groundmass mainly composed of sanidine and anorthoclase laths ($An_{0-11}Ab_{32-70}Or_{21-67}$), tiny Fe–Ti oxides and green interstitial ferro-hedenbergite (15 modal %; $En_2Wo_{42}Fs_{56}$; Fig. 4IIb). The latter occurs either in association with the groundmass feldspar (Fig. 5b) or as euhedral to subhedral crystals on the walls of most of the vesicles (also together with zircon; Fig. 5c). Rare microphenocrysts with ferro-augitic cores ($Wo_{45}En_{26}Fs_{29}$), similar to those found in the syenites, and green ferro-hedenbergite rims ($Wo_{43-42}En_{8-2}Fs_{49-56}$) are also present (Fig. 5d).

A massive porphyritic lava flow (sample PAT-27), sampled close to Pico Rojo neck, is characterized by phenocrysts of quartz (5> modal %), homogeneous ferroaugite (5 modal %, $En_{24}Wo_{39}Fs_{37}$; Fig. 4IIb), zoned anorthoclase (15 modal %; $An_{34-5}Ab_{46-77}Or_{6-39}$; Fig. 4Ib), Fe–Ti oxides (10 modal %) and accessory subhedral apatite set in an oriented (trachytic) alkali feldspar-lath groundmass (Fig. 4Ib).

7. Geochemistry

A total of seven samples were analyzed for major and trace elements and six for Sr and Nd isotopes. The corresponding data set is presented in Tables 3 and 4. Data for the post-plateau basalts of the MLBA (Baker et al., 1981; Gorring et al., 2003; Guivel et al., 2006) as well as those from the 3.2 Ma old Las Nieves pluton (Morata et al., 2002) were also plotted in all geochemical diagrams (Figs. 6–9).

7.1. Major and trace elements

SiO_2 concentrations of analyzed rocks range from 60 to 68 wt.%, with Cerro Lápiz alkali microgranite (PAT-12) being the more silica-rich sample. A marked SiO_2 gap (from 52 to 61 wt.% SiO_2) separates the Pliocene felsic alkaline volcanism from the contemporaneous post-plateau basalts, as expected in a typical bimodal suite.

In the total alkalis vs. silica diagram (Fig. 6) the western MLBA Pliocene felsic sub-volcanic rocks and lava flows plot in the trachyandesite (syeno-diorite), trachyte (syenite) and alkali rhyolite (alkali granite) fields. In the Na_2O vs. K_2O diagram shown in Fig. 6 they plot in the potassic field ($Na_2O/K_2O = 0.9–1.48$; average 1.16), differing therefore from coeval post-plateau basalts which mainly plot in the Na-series field. All the felsic rocks are mainly peraluminous to slightly metaluminous (A/CKN = 1.05–0.97) and quartz-normative (CIPW norm) in contrast with the undersaturated, nepheline-normative post-plateau basalts. All the intrusives classify as "within plate granitoids" in the

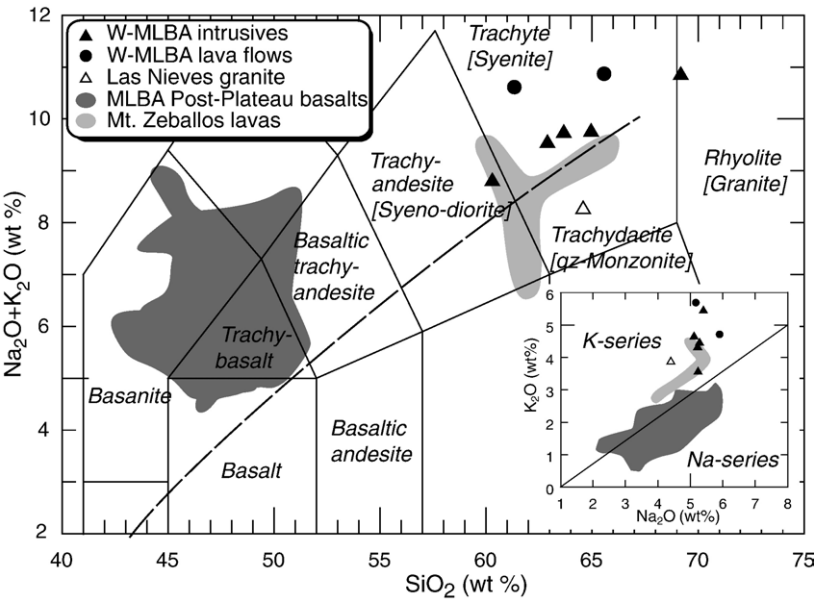

Fig. 6. Total alkali vs. silica (TAS) classification diagram (Le Bas et al., 1986) for the Pliocene magmatic rocks of Meseta del Lago Buenos Aires. The corresponding plutonic rock names for each field are shown between brackets. Filled triangles: western MLBA intrusives, open triangle: Las Nieves quartz-monzonite, filled circles: western MLBA lava flows. Inset: Na_2O vs. K_2O subdivision diagram of the alkaline series (Middlemost, 1975). The fields of MLBA Pliocene Post-Plateau basalts (Baker et al., 1981; Gorring et al., 2003; Guivel et al., 2006) and Mt. Zeballos alkaline rocks (Dasilva et al., 2006) are also shown. Division line between alkaline and sub-alkaline series from Irvine and Baragar (1971).

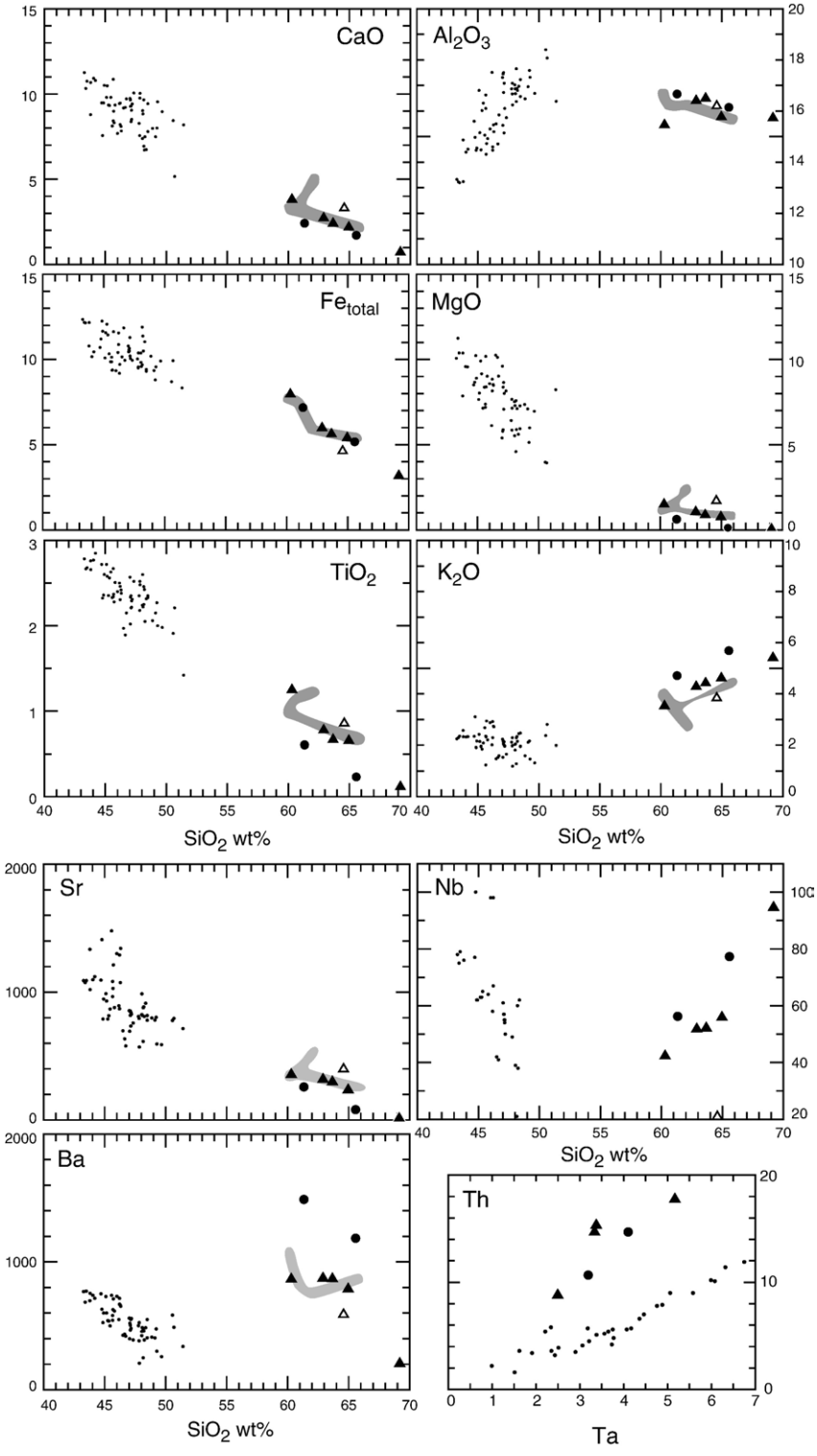

Fig. 7. Selected major (wt.%) and trace elements (ppm) vs. SiO_2 together with Ta vs. Th rectangular diagrams for W-MLBA felsic rocks. MLBA Pliocene post-plateau basalts (black dots: Baker et al., 1981; Gorring et al., 2003; Guivel et al., 2006) and the field (light grey) of some Mt. Zeballos alkaline rocks (Dasilva et al., 2006) are also shown. Data re-calculated on a water-free basis. Symbols as in Fig. 6.

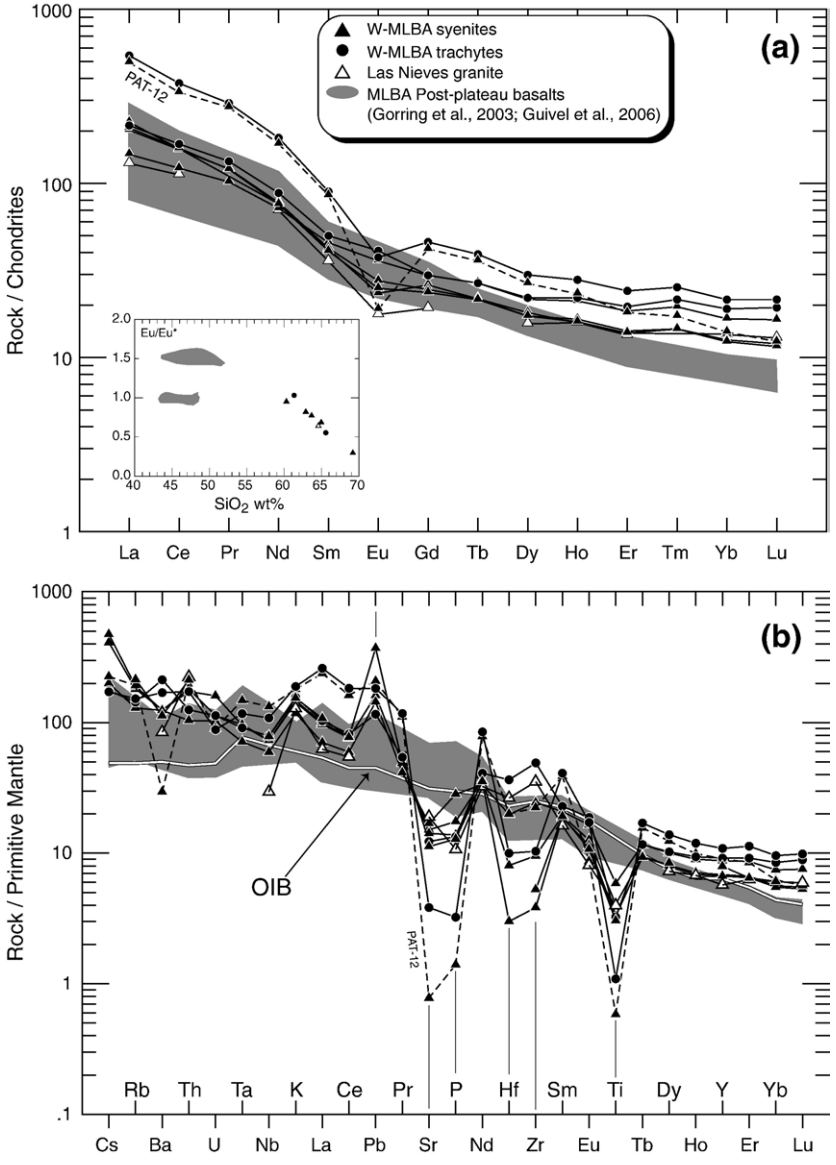

Fig. 8. a) Chondrite-normalized REE diagram (Nakamura, 1974) for Pliocene W-MLBA felsic rocks. Inset: diagram showing positive correlation between the extent of the negative Eu anomaly and SiO_2 wt.%. b) Primitive mantle-normalized trace elements diagram (Sun and McDonough, 1989; plus Ta and Hf from Wedepohl and Hartmann, 1994) for W-MLBA felsic rocks. The field for MLBA Pliocene post-plateau basalts (Gorring et al., 2003; Guivel et al., 2006) is shown in dark grey. Open triangle: Las Nieves quartz-monzonite (Morata et al., 2002). Dashed line in both diagrams is for Cerro Lápiz sample (PAT-12).

granitoid discrimination diagrams of Pearce et al. (1984) (e.g. Y+Nb vs. Rb), as "A-type granites" in the 10 000×Ga/Al vs. Zr+Nb+Ce+Y diagram of Whalen et al. (1987) and in the "A_1-type" subdivision of A-type granitoids of Eby (1992) (not shown).

Selected major (wt.%) and trace elements (ppm) vs. silica (wt.%) variation diagrams are shown in Fig. 7. CaO, Fe_{total}, TiO_2 (Fig. 7) and MnO, P_2O_5 (not shown) show negative correlations with SiO_2, in the prolongation of the trends defined by the MLBA post-plateau basalts. Contrarily, K_2O shows a positive correlation with SiO_2, and MgO and Al_2O_3 display weak negative trends different from those defined by the post-plateau basalts, which are either positively (for Al_2O_3) and strongly negatively (for MgO) correlated with SiO_2. Nb (Fig. 7), Ta, Th and Rb (not shown) behave incompatibly in the felsic rocks, showing positive correlations with SiO_2, different from the post-plateau basalt trends. Sr and Ba

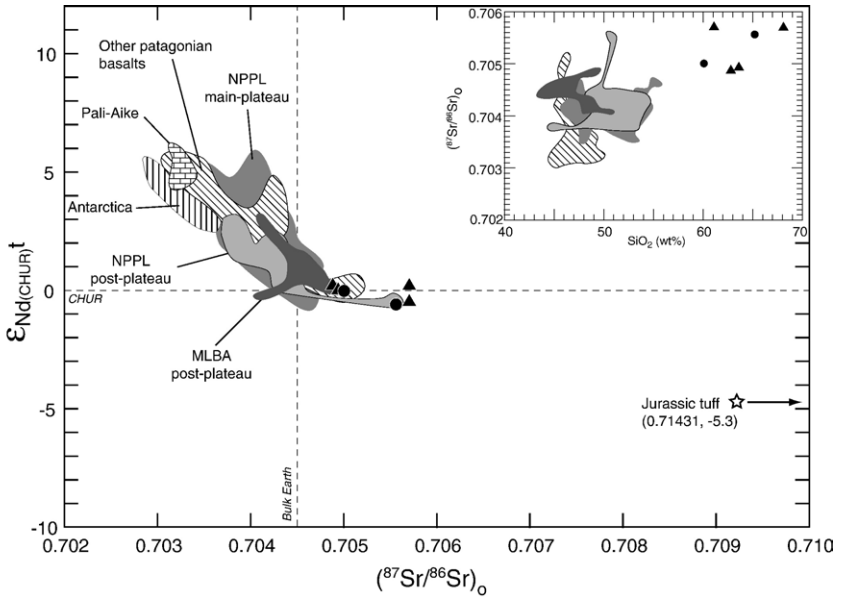

Fig. 9. a) $(^{87}Sr/^{86}Sr)_o$ vs. εNd diagram for Pliocene W-MLBA alkaline rocks. Initial isotopic ratios of rocks older than 3 Ma (plotted for comparison) were re-calculated at 3 Ma. MLBA post-plateau basalts from Hawkesworth et al. (1979) and Gorring et al. (2003). Other Neogene slab window-related lavas from Antarctic Peninsula (Hole et al., 1995), Pali-Aike (D'Orazio et al., 2000, 2001), and the Neogene (main- and post-plateau) Patagonian Plateau Lavas province (NPPL, Stern et al., 1990; Gorring et al., 1997; Gorring and Kay, 2001) are also plotted. Star symbol: Jurassic (160 Ma) rhyolitic tuff (Parada et al., 2001). Symbols as in Fig. 8.

display poor negative correlations with SiO_2; notably, Cerro Lápiz microgranite sample shows very low contents in Ba and Sr. In contrast, all incompatible trace elements in the post-plateau basalts show negative correlations with silica contents, evidencing variable partial melting degrees of a primitive mantle source (Guivel et al., 2006) (Fig. 7). In rectangular diagrams, strongly incompatible elements (e.g. Ta vs. Th; Fig. 7) define diverging trends passing through the origin for mafic and felsic rocks. Some compatible elements such as Sc and V display a negative correlation with SiO_2 (not shown). Other compatible trace elements such as Co, Cr, Ni have very low concentrations in the felsic rocks, close to analytical detection limit.

All the studied felsic rocks are enriched in Light Rare Earth Elements (LREE) ($(La/Sm)_N$ = 3.2–6.0; $(La/Yb)_N$ = 8.8–16.9, up to 35.4 in sample PAT-12; Fig. 8a), with LREE fractionation increasing with SiO_2 content. All but Cerro Lápiz alkali microgranite sample (PAT-12) exhibit sub-horizontal Heavy REE (HREE) patterns ($(Dy/Yb)_N$ = 1.16–1.40), contrasting with the fractionated HREE patterns of the coeval post-plateau basalts. This sample (PAT-12) shows a slightly fractionated HREE pattern ($(Dy/Yb)_N$ = 1.90) which results in a HREE trend sub-parallel to those of post-plateau basalts. All the studied felsic rocks show a negative Eu anomaly (Eu/Eu* = 0.3–0.9), the importance of which correlates positively with SiO_2 contents (Fig. 8a): the lowest Eu/Eu* (0.3) is observed in the most evolved rock (sample PAT-12, 68.1 wt.% SiO_2).

Primitive mantle-normalized spider diagrams (Fig. 8b) for the studied rocks show similarities with those of OIB-like post-plateau basalts (Gorring et al., 2003), together with strong negative anomalies in some elements. All the felsic rocks display similar and sub-parallel patterns enriched in Large Ion Lithophile Elements (LILE; e.g. Rb = 82–122 ppm; Ba = 790–1488 ppm). They are variably depleted in High Field Strength Elements (HFSE; e.g. Ta, Nb, Hf, Zr, Ti) as well as in Sr and P, and enriched in Pb. Cerro Lápiz alkali microgranite and the associated trachyte (samples PAT-12 and -13, respectively) are particularly enriched in LREE and Th and depleted in U, Sr, P and Ti, far below the concentrations in the other acid rocks.

7.2. Sr–Nd isotopes

The Sr and Nd isotopic compositions measured in six felsic samples from the western MLBA are reported in Table 4 and plotted in Fig. 9. All the analyzed samples plot in the Mantle Array, with $(^{87}Sr/^{86}Sr)_o$ values ranging from 0.70488 to 0.70571 and $(^{143}Nd/^{144}Nd)_o$

from 0.512603 to 0.512645 (εNd = 0.2 to −0.6), defining a clear trend rooted in the field of the MLBA post-plateau basalts. A positive correlation between SiO_2 (wt.%) content and $(^{87}Sr/^{86}Sr)_o$ (and negative with respect to εNd_o) is observed. Within this trend, three of the analyzed rocks have Sr and Nd isotopic ratios similar to those of the coeval post-plateau basalts (Fig. 9). Samples from Cerro Lápiz area (PAT-12 and -13) and Pico Rojo neck (PAT-29) plot outside this field, having the most enriched Sr isotopic signature ($(^{87}Sr/^{86}Sr)_o$ = 0.70556–0.70571) and depleted Nd isotopic signature ($(^{143}Nd/^{144}Nd)_o$ = 0.512603–0.512608 with εNd = −0.5 to −0.6) of all reported rocks from the MLBA.

8. Discussion

The main petrogenetic problems which arise from the study of bimodal volcanic provinces are related to the origin of the alkaline felsic rocks, their relationships with coeval basaltic magmatism and the explanation of the lack of rocks having intermediate compositions (see Peccerillo et al., 2003 and references therein). In the particular case of the Pliocene MLBA magmatism, additional important issues are i) its relationships with slab tear/window processes, ii) the origin of the alignment of the felsic intrusions along the Zeballos Fault Zone, and iii) its relationships with the Mio-Pliocene tectonic evolution of the area.

8.1. Origin of felsic alkaline magmas

Two main hypotheses have been proposed to explain the genesis of bimodal alkaline magmatism. One states a genetic relationship between mafic (mantle-derived) and felsic rocks through fractional crystallization processes with variable (or even absent) crustal contamination (AFC process) (Litvinovsky et al., 2002; Mingram et al., 2000; Peccerillo et al., 2003;Vernikovsky et al., 2003; Wang et al., 2005). The other hypothesis invokes the genesis of mafic and felsic magmas from different sources, the felsic melts being generated either from the anatexis of crustal country rocks or from the partial melting of young underplated basalts (Whalen et al., 1987; Tchameni et al., 2001), and the basic rocks derived directly from mantle partial melting. For the Plio-Pleistocene undersaturated alkaline and primitive MLBA post-plateau basalts, Gorring et al. (2003) and Guivel et al. (2006) proposed a genesis from an OIB-type asthenospheric source, variably contaminated by an EM1-type component from the Patagonian lithospheric mantle. Therefore, the two main hypotheses described above for the genesis of coeval silica-oversaturated felsic magmas will be tested in the framework of this genetic model for the mafic lavas.

8.1.1. Melting of basement rocks or underplated basalts

The basement rocks exposed along the western flank of the MLBA, below the ~600 m thick Miocene molasse, correspond to the more than 1000 m thick Early Jurassic–Early Cretaceous ignimbrites and rhyolites of the Ibáñez Group, and, to the west, to the Eastern Andean Metamorphic Complex (EAMC, Fig. 2a). Sr and Nd isotopic ratios of Middle Jurassic rhyolitic tuffs are around $^{87}Sr/^{86}Sr$ = 0.714405, $^{143}Nd/^{144}Nd$ = 0.512362 (Parada et al., 2001) and the average of the Patagonian S-type crust is $^{87}Sr/^{86}Sr$ = 0.72184, $^{143}Nd/^{144}Nd$ = 0.51232 (Kilian and Behrmann, 2003), which could be representative of the isotopic signature of the EAMC. As Sr and Nd isotopic ratios of western MLBA felsic rocks are less and more radiogenic, respectively, than these possible crustal sources (see Table 4), derivation by melting of these basement rocks is not supported by our isotopic data. Additionally, ratios of incompatible elements such as LILE/HFSE ratios (e.g. Rb/Nb, Rb/Zr, Th/Ta) should remain constant or increase in liquids formed by melting of crustal rocks, as LILE are more incompatible than HFSE during crustal anatexis (e.g. Ayers and Harris, 1997). The studied rocks have LILE/HFSE ratios (e.g. Rb/Nb = 1.3–2.4; Ba/Nb = 2.2–27) lower than the Jurassic volcanics (Rb/Nb = 6.1–24; Ba/Nb = 96–218) and the metamorphic basement (Ba/Nb = 11.2–53, Faúndez et al., 2002; Rb/Nb = 7, Ba/Nb = 34, Kilian and Behrmann, 2003). Hence, there are neither isotopic nor incompatible trace element arguments supporting the derivation of the alkaline felsic magmatism of the MLBA from anatectic processes involving the basement rocks.

On the other hand, some of the alkaline felsic rocks from the western MLBA have Sr and Nd isotopic signatures similar to those of the post-plateau MLBA basalts (Fig. 9). This feature could be consistent with a model of genesis of the evolved magmas through partial melting of underplated basalts with isotopic compositions similar to those of the post-plateau basalts. The HREE patterns and high Yb_N values (>10) of the studied felsic lavas seem to exclude the presence of garnet as an important residual phase in their source, which could be consistent with the "normal" thickness of the Central Patagonia crust (<40 km; Introcaso et al., 1996; Tassara et al., 2006). Indeed, garnet is only stable in meta-basaltic amphibolites at pressures higher than 0.9 GPa (Schmidt and Poli, 1998). Therefore the generation of the studied felsic lavas through partial melting of OIB-type underplated basalts has been tested

by incompatible and compatible trace element modeling in Section 8.1.3. However, this hypothesis cannot explain the high Sr and low Nd isotopic ratios of the alkali microgranite and related trachyte, and the occurrence of an additional open-system process has to be considered as discussed below.

8.1.2. Fractional crystallization of alkali basaltic magmas

Numerous evidences are found in the petrography and chemistry of the analyzed samples that support mineral fractionation of a basaltic melt as the main driving mechanism to explain the differentiated signature of western MLBA felsic rocks.

The behavior of elements such as MgO, Al_2O_3, K_2O, Sc and V is that expected for a series evolving through fractional crystallization of the mineral phases observed in the analyzed samples. Depletions in Sr, P, Hf, Zr and Ti might be explained as a consequence of fractionation of plagioclase, apatite, zircon and Fe–Ti oxides, respectively. The variable Ce/Pb ratios (Table 3) of the less evolved felsic samples could trace either mineral fractionation effects or contamination by a low Pb/Ce assimilant (Section 8.1.3); but the extreme Ce enrichments (highest Ce/Pb ratios) observed in the most evolved rocks might be a consequence of the crystallization of LREE-bearing minerals (see below). The TiO_2 contents of all our samples do not correlate with Zr and Hf values, implying that the latter were not controlled by fractionation of Ti-oxides, but rather by the removal of zircon, which is an accessory phase in many samples. Especially, Mifeldi syenitic samples (PAT-20 and -22) are depleted in Zr and Hf (59 and 43 ppm Zr; 1.022 ppm Hf) compared to the other analyzed rocks (116–550 ppm Zr; 3.4–12.4 ppm Hf) reflecting intense zircon fractionation in these magmas. The concentrations of trace elements compatible with respect to feldspar (Ba, Sr, Eu) are also variable, particularly in Cerro Lápiz samples, which display the lowest Ba and Sr contents of our set (206 ppm Ba; 16 and 81 ppm Sr; Figs. 7 and 8b) and are the only rocks having sanidine as an early phase. Furthermore, the increase of the Eu anomaly with magmatic differentiation, together with the good correlation of Eu/Eu∗ with Sr, and the lack of it with Ba, suggest that low-pressure fractionation of plagioclase was predominant over that of alkali feldspar. Fractionation of clinopyroxene and Fe–Ti oxides is evidenced by strongly decreasing Sc and V contents as silica increases among the felsic rocks. It is well-known that the crystallization of accessory mineral such as allanite and monazite in metaluminous to peralkaline granitic melts strongly fractionates LREE from HREE (e.g. $(Dy/Yb)_N^{allanite} = 1.36–5–56$; Poitrasson, 2002), Th from U and typically produces a pronounced negative Eu anomaly in chondrite-normalized diagrams (see Gieré and Sorensen, 2004, and references therein). Therefore, the extremely fractionated REE patterns of the most evolved rocks (e.g. PAT-12, $(La/Yb)_N = 35$; $(Dy/Yb)_N = 1.9$) and the variable enrichments in other trace elements (Fig. 8) are at least partly explained by the precipitation of these incompatible element-rich minerals (see Section 6.1). All these observations are consistent with the genesis of felsic rocks through low-pressure fractional crystallization of mafic magmas in shallow crustal chambers, providing wide opportunity for assimilation, and they further imply that the Cerro Lápiz microgranite is more fractionated than the rest of our sample set.

Regarding the genetic relationships between mafic and felsic rocks, the huge volumetric dominance of basalts over the latter also favors the fractional crystallization hypothesis (with or without assimilation) as the main viable mechanism to explain the Pliocene bimodality of the MLBA rocks. However, this hypothesis fails to explain the lack of intermediate rocks, which remains a problem for many bimodal alkaline provinces (Peccerillo et al., 2003).

8.1.3. Closed vs. open-system evolution: AFC model for MLBA felsic rocks

Augite syenites, commonly present in alkaline intrusive complexes, are often associated with alkali granites, together with more evolved or cumulate rocks (Greenland, Stevenson et al., 1997; South China, Wang et al., 2005; Southern Brazil, Gualda and Vlach, 2006; India, Upadhyay et al., 2006; among others). In Central Patagonia this typical lithologic association occurs almost synchronously (Mifeldi augite-microsyenite: 3.08-3.28 Ma; Cerro Lápiz alkali microgranite: 3.65 Ma), but more differentiated rocks and/or cumulates are lacking or are not yet recognized. Many authors have postulated a genetic relationship among these lithotypes, the alkali granites being produced through fractional crystallization ± assimilation of alkali basaltic or augite syenitic liquids (Stevenson et al., 1997; Marks and Markl, 2001; Litvinovsky et al., 2002).

Closed system fractional crystallization from one of the most primitive MLBA post-plateau basalt taken from Gorring et al. (2003) has been tested by simple mass balance calculations using major elements. Mineral compositions measured by Espinoza et al. (2005a) in similar basalts from Meseta Chile Chico were used in this model. To obtain the composition of the less evolved syenitic rock (sample PAT-29), an assemblage consisting of 23 wt.% olivine, 48 wt.% plagioclase, 21.5 wt.% clinopyroxene, 5.8 wt.% of magnetite and

1.8 wt.% apatite needs to be removed through a high rate of fractional crystallization ($\Sigma r^2 = 1.54$). Then, mass balance calculations allow modeling major element behavior between sample PAT-29 and the more evolved (and younger) PAT-20 microsyenite. For this pair, a fractionating assemblage of 56.5 wt.% plagioclase, 24.6 wt.% clinopyroxene, 16.5 wt.% magnetite and 2.4 wt.% apatite is needed ($\Sigma r^2 = 0.46$). To better constrain this hypothesis, trace element closed system fractional crystallization modeling was carried out yielding reasonable, but not well-fitted results (see Fig. 10a and b and Table 5).

The behaviors of both incompatible and compatible elements were tested to further confirm the results of the above models, and to evaluate a hypothetical genesis of the felsic rocks by partial melting of either a basaltic source (underplated basalts) chemically equivalent to the MLBA post-plateau ones, or a more evolved rock derived from the fractionation of primitive basalts. In the models carried out using highly incompatible elements (e.g. Th vs. La; Fig. 10b), neither closed system fractional crystallization (CSFC) nor partial melting (PM) from a chemically equivalent primitive source reproduce the chemical composition of felsic rocks. In models using highly compatible elements (Cr vs. Th; Fig. 10c) a rather satisfactory fit is observed only for the CSFC model. For moderately compatible elements (e.g. Sc vs. La; Fig. 10d), the CSFC model yields rather satisfactory results only for some of the less evolved samples. Similarly, PM calculations starting from a more evolved basaltic source fail to reproduce consistently the enrichments observed in some samples. These results are consistent with the fact that PM processes generates liquids with variable enrichments in incompatible elements but with moderate depletion in compatible elements, while CSFC is much more efficient in producing compatible elements depletion than incompatible elements enrichment. Therefore, a

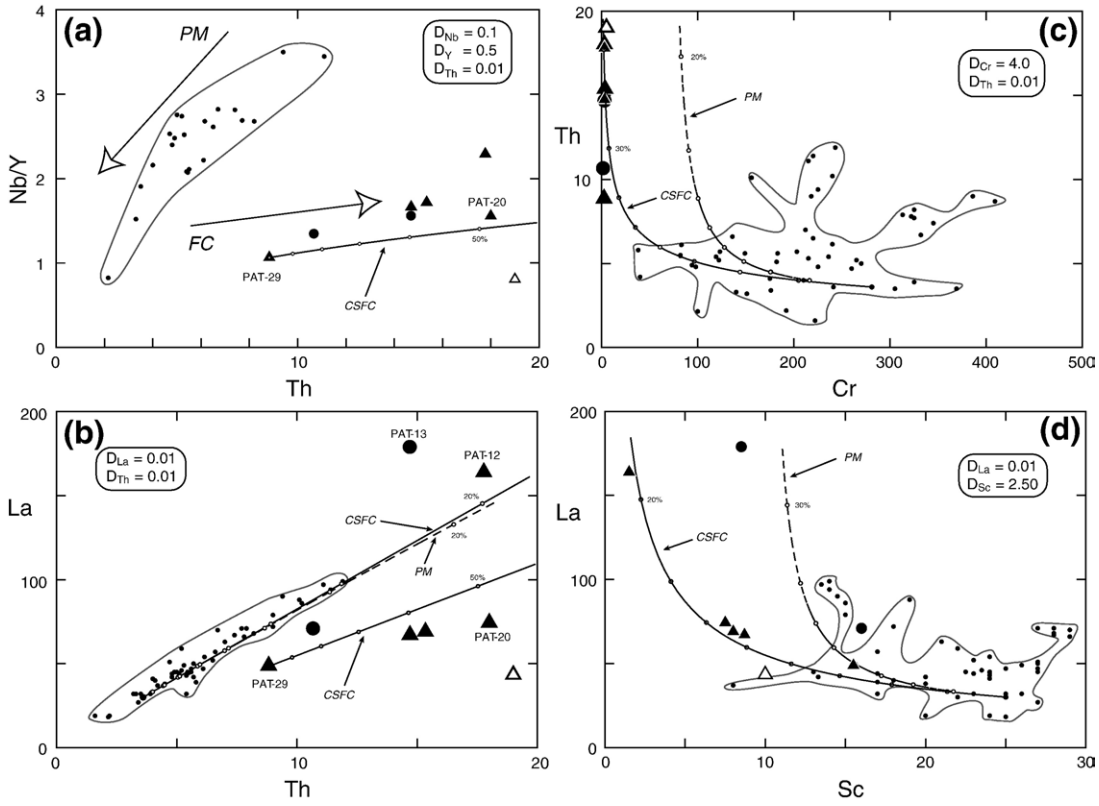

Fig. 10. Variation diagrams illustrating partial melting (PM, dashed line) and closed system fractional crystallization (CSFC, continuous line) models applied to trace elements for the W-MLBA felsic rocks. a) Th vs. Nb/Y diagram showing that CSFC processes starting from the less evolved syenite (PAT-29) could partially reproduce the values observed in the more differentiated samples; b) Th vs. La diagram showing that the high HFSE enrichments of felsic rocks cannot be achieved either by CSFC or by PM of a primitive basaltic source; and alternative CSFC model showing that only part of the studied rocks could be generated starting from the less evolved syenite; c) Cr (compatible) vs. Th diagram evidencing good CSFC model fit; d) Sc (moderately compatible) vs. La diagram showing a loose fit for the CSFC model. Bulk distribution coefficients (*D*) used for each model are indicated in the corresponding diagram. Ticks every 10% in model lines represent amount of melt. See text for discussion.

Table 5
Parameters used in CSFC and AFC models in Figs. 7, 10 and 11

Sample	AP-02s	120395-10	EAMC	S-type crust	PAT-29
Rock type	Alkali basalt	Tuff	Limestones–sandstones		Microsyenite
Role	Parental magma	Assimilant	Assimilant	Assimilant	Parental magma
Age [Ma]	3.4>	160	Paleozoic	Paleozoic	3.08
Cr (ppm)	281				
D_{Cr}	4				
Sc (ppm)	25				
D_{Sc}	2.5				
Ba (ppm)	419	1810	304	482	
Nb (ppm)	–	8.3	10	14.3	42.4
High D_{Nb}					0.1
Low D_{Nb}					0.02
Ta (ppm)	2.35				
D_{Ta}	0.01				
Y (ppm)					39.8
High D_Y					0.5
Low D_Y					0.1
Th (ppm)	3.6				8.83
D_{Th}	0.01				0.01
Rb (ppm)	–	94	–	101.0	
Sr (ppm)	579.0	117	80.0	173.0	
High D_{Sr}	3.0				
Low D_{Sr}	1.1				
La (ppm)	30.0				48.4
D_{La}	0.01				0.01
Sm (ppm)	5.80	4.4	6.00	6.00	
Nd (ppm)	30.00	28.9	30.00	28.60	
$^{87}Sr/^{86}Sr$	0.704597	0.71441		0.72184	
$(^{87}Sr/^{86}Sr)_o$	0.704597	0.71431			
$^{143}Nd/^{144}Nd$	0.512708	0.512362		0.51232	
$(^{143}Nd/^{144}Nd)_o$	0.512706	0.512360			
$eNd_{CHUR(3\ Ma)}$	1.4	−5.3			

EAMC: Eastern Andean Metamorphic Complex.
D: magma distribution coefficient for indicated element.
–: no data.
Jurassic tuff from Parada et al. (2001); Pliocene alkali basalt from Gorring et al. (2003).
Values for EAMC and S-type crust are averages from Faúndez et al. (2002) and Kilian and Behrmann (2003).

derivation of the felsic rocks through fractional crystallization of primitive basaltic magmas is favored. The contrasted behavior of highly (Cr) and moderately (Sc) compatible elements indicates that high amounts of olivine, rather than clinopyroxene, were removed from the basaltic liquids, a feature consistent with the petrography of post-plateau olivine-rich basalts.

Finally, it is necessary to call for open-system models to justify some high incompatible elements concentrations (Fig. 10a and b) as well as the Sr and Nd isotopic signatures of the more evolved magmas (Fig. 9). AFC models according to DePaolo (1981) were tested using the same primitive basaltic source and choosing as an assimilant a Middle Jurassic rhyolitic tuff from the Ibáñez Formation (sample 120395-10 outcropping 20–25 km southwest of the studied area: $^{87}Sr/^{86}Sr=0.714405$, $^{143}Nd/^{144}Nd=0.512362$; Parada et al., 2001, Table 5). These AFC tests show that the genesis of the complete suite of felsic rocks from the W-MLBA requires ratios of assimilation vs. crystallization (*r*) lower than 0.3 and progressively increasing D_{Sr} during fractionation. According to the Sr vs. $(^{87}Sr/^{86}Sr)_o$ model (Fig. 11a), the composition of the less evolved acid rock (PAT-29) is obtained for *F* values (amount of residual liquid) between 30–40%, a *r* value of ~0.30 and a low $D_{Sr}=1.1$, otherwise unrealistic *r* values as high as 0.9 are needed (Fig. 11a, curve 1). Mifeldi microsyenites and dyke (PAT-20, -22 and -21) need *F* values between 30 and 70%, with *r* values between 0.10–0.30 and $D_{Sr}=1.5$–2.0 (Fig. 11a, curves 2, 3 and 4). The highly differentiated alkali microgranite (PAT-12) and the associated trachytic lava (PAT-13) require the highest amount of crystallization

(F=15–20%), an even lower range for r=0.03–0.10 and higher values for D_{Sr}=2.0–3.0 (Fig. 11a, curves 3 and 5). These results are corroborated when the model is tested with incompatible elements ratios (La/Nb vs. Sr/La; Fig. 11b, curve 1) and also when strongly incompatible trace elements (e.g. Ta) concentrations are modeled (Fig. 11).

Following the major element modeling results, another tested model was the derivation of the alkali microgranite and related trachyte by AFC of the less evolved syenite (PAT-29), using the same assimilant (Middle Jurassic rhyolitic tuff) composition. This model might explain the existence in the trachytic lava of clinopyroxene cores with compositions similar to those of the syenites (Figs. 4IIb, 5d). The same type of Sr isotopic model (not shown) yields satisfactory results for similar low r values (0.02–0.1), but with slightly higher F=25–55% and also only for D_{Sr} as high as 3. In addition, equivalent modeling using trace elements also indicates that low r values (0.1) and high D_{Sr} (~3) are required to generate the most differentiated magmas (Fig. 11b, curve 2). To comply with some of the above models, assuming a compatible behavior for Sr (D_{Sr}=3) is necessary. Peccerillo et al. (2003) showed that, although values of D_{Sr}=3 are somewhat higher than those found in alkali basalts, these values are rather optimal for felsic systems in which feldspar is the dominant fractionating phase, as it is the case here.

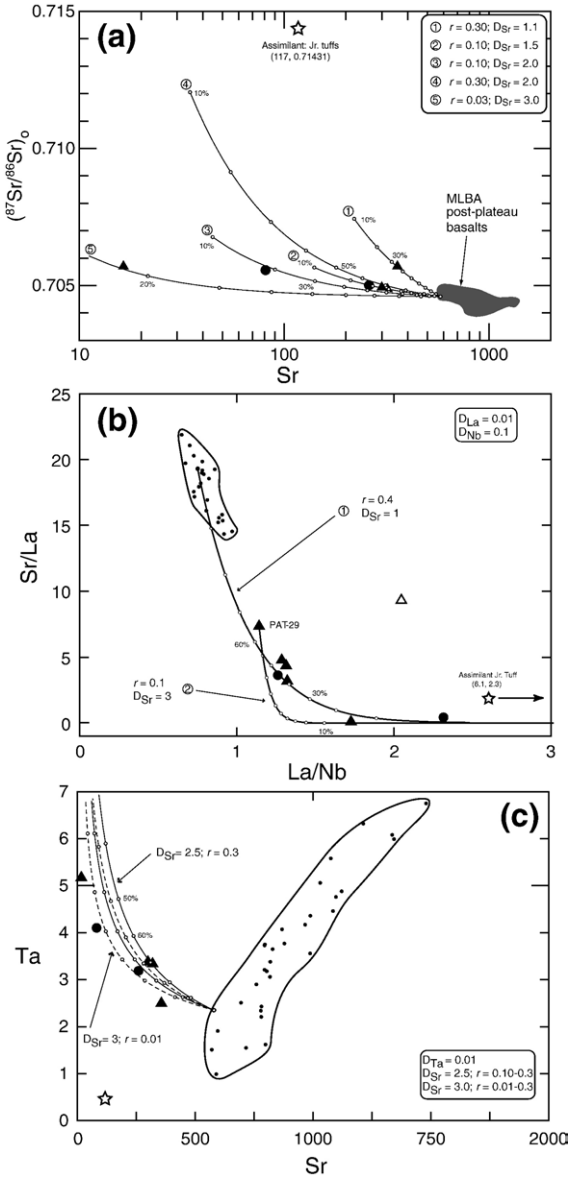

Fig. 11. a) Assimilation–fractional crystallization (AFC) modeling showing that Sr contents and the Sr isotopic signature of W-MLBA felsic rocks can be achieved by ratios of assimilation of the country rocks (Jurassic tuffs) vs. crystallization (r) lower than 0.4 and progressively increasing D_{Sr} during fractionation of a primitive post-plateau basaltic liquid (curves 1 to 4). That of the more differentiated Cerro Lápiz rocks needs even lower rates of assimilation/fractional crystallization but higher crystallization rates (curve 5, r=0.03–0.1; F=~15%); b) equivalent AFC model applied in a La/Nb vs. Sr/La diagram; curve 1: starting from the same basaltic source in a) to yield the ratios of the other samples using similar parameters (r and D_{Sr}); curve 2: alternative AFC model for the generation of the most differentiated magmas starting from the less evolved syenite (PAT-29) with F values<10%, and also low r values (0.1) and high D_{Sr} (3), c) equivalent AFC modeling of an strongly incompatible element (Ta) in the felsic rocks, corroborating results shown in a) and b). Ta value for the Jurassic tuff calculated as Ta*=Nb/17. Star symbol: Jurassic tuff from Ibáñez Formation used as assimilant. Bulk distribution coefficients (D) used for each model are indicated in the corresponding diagram. Ticks every 10% in model lines represent amount of residual liquid (F). See text for discussion.

8.2. Proposed petrogenetic model

The geochemistry of the MLBA OIB-type post-plateau basalts supports an origin by low degrees (1–5%) of partial melting of a peridotitic primitive mantle source in the garnet stability field (65–70 km), and interaction with the Patagonian continental lithospheric mantle to gain their enriched isotopic signature (Gorring et al., 2003). The mechanism for melting is thought to be the decompressional melting of upwelling subslab asthenospheric material due to the generation of a slab window in the subducting plate, as a consequence of either the subduction of diverging segments of the active Southern Chile Ridge (Gorring et al., 1997; Gorring and Kay, 2001; Gorring et al., 2003; Espinoza et al., 2005a) or the opening of a slab tear parallel to the trench during ridge-trench collision (Guivel et al., 2006).

Models based on Sr–Nd isotopes and major and trace elements indicate that Pliocene felsic rocks from the western MLBA area could be generated by AFC processes of coeval post-plateau basaltic liquids contaminated in upper crustal levels by Jurassic ignimbrites of the Ibáñez Formation. In all tested models the Cerro Lápiz alkali microgranite and the associated trachytic lava (samples PAT-12 and -13) need a very high degree of fractional crystallization to achieve their elemental and isotopic signatures. Similarly, Stevenson et al. (1997) noted that the genesis of alkaline granite in the Ilímaussaq Complex probably occurred through large-scale contamination and crystallization of basaltic or augite syenite magmas. The fractional crystallization hypothesis is able to explain most of the geochemical and isotopic features of the mafic–felsic MLBA suite, but it implies the need for large volumes of basaltic magmas to generate the felsic melts by this process. In this respect, the volume estimate of ~ 600 km^3 (Gorring et al., 2003) for the MLBA post-plateau lavas and cones is clearly much higher than the ~ 0.5 km^3 minimum estimated volume of the felsic intrusions. This, together with the low assimilation rates calculated, is consistent with the results of Dufek and Bergantz (2005) who showed the difficulty to generate large amounts of crustal melts based on thermal input (mantle melts) and crustal thickness constraints.

Consequently, a two stage petrogenetic model can be proposed for the genesis of the felsic magmatism in the western border of the MLBA. In its first step, enriched asthenospheric basaltic melts were generated from mantle upwelling and ascended through a slab tear or window, forming the MLBA post-plateau sequence (Gorring et al., 2003; Guivel et al., 2006). Second, part of these magmas was stored in shallow level intracrustal magma chambers, where intense fractionation of plagioclase, clinopyroxene, Fe–Ti oxides, apatite, zircon (see Section 8.1.2), together with minor assimilation of host Jurassic felsic volcanics, generated the evolved liquids. The first mantle-derived magmas interacted with the host rocks (high r values) and stayed in the magma chamber, allowing extensive fractional crystallization which generated the less evolved syenitic liquids (now the Mifeldi and Pico Rojo syenites and trachytes). Continuously, newly injected primitive melts mixed with mafic magmas ponding at the bottom of the chamber. Later, an increase in mineral fractionation rate (low r values), now dominated by feldspars (as evidenced by chemistry and texture of samples PAT-12 and -13), together with a decrease in assimilation rates of the wall rock (now less fertile), generated low density-highly differentiated granitic magma (now the Cerro Lápiz alkali microgranite and trachytes). This hypothesis is also coherent assuming that granitic melts derive from parental syenitic melts (see Section 8.1.3). Then, Fe- and Zr-rich residual magmatic liquids re-equilibrated with the felsic melts and precipitated Fe-rich clinopyroxenes and zircons in the interstices of the main mineral framework and in volatile-filled vesicles. Later, mafic magmas ponding near the bottom of the partly emptied magma chamber may have used the same structures that the felsic liquids and/or ancient structures to reach the surface. Finally, younger mantle-derived mafic melts may have reached directly the surface without shallow storage, and were emplaced during the Pleistocene in the eastern part of the MLBA (Fig. 12).

The intrusion sequence is constrained by the ages we obtained (Table 1) and is consistent with the temporal evolution of a zoned magma chamber, further supporting the AFC model discussed above. The first generated syenitic magmas intruded north of the studied area (Pico Rojo neck); later, granitic magmas stored in the upper part of the magma chamber, generated from either newly injected mafic magmas or older remnant syenitic liquids, intruded the southern part of the Zeballos Fault Zone (Cerro Lápiz neck); and finally, syenitic magmas coming from deeper levels in the magma chamber reached sub-volcanic depths (Mifeldi laccolith and dykes; Figs. 2b and 12). Simultaneously, scarce trachytic lava flows were emplaced at the surface.

A stratified magma evolution in a shallow magmatic reservoir (e.g. Turner and Campbell, 1986; Peccerillo et al., 2003) like that described above could explain the lack of rocks with intermediate compositions (the Daly gap). Low density and crystal-rich differentiated (and assimilated) liquids accumulated at the top of the chamber, acting as a barrier for deeper basaltic magmas to undergo convective stirring. Furthermore, the recurrent injection and mixing with asthenospheric melts may have prevented differentiation of mafic magmas in the deep layers of the chamber. Therefore, a well-stratified reservoir could be able to avoid (or restrict) the generation of liquids with intermediate compositions. As no other felsic rocks with crystallization ages younger than those described here have been reported for the MLBA, we may suppose that this process of differentiation occurred once at the beginning of post-plateau magmatism. Therefore, the studied felsic magmas could have frozen at shallow levels below the volcanic system developed in the western edge of the MLBA, preventing the extrusion of their parental mafic magmas. This could have resulted into an eastward migration of volcanic activity, as evidenced by the occurrence of Pleistocene–Holocene basaltic cones and

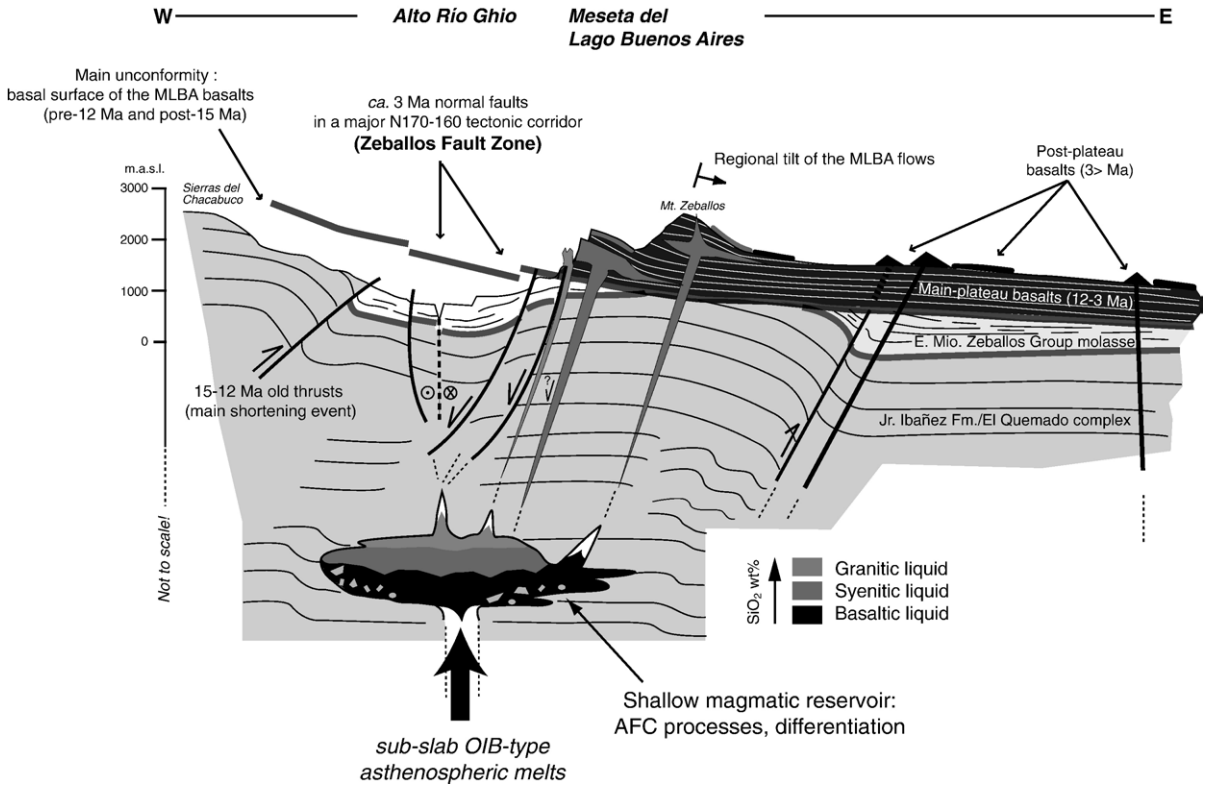

Fig. 12. Actual schematic WE section across the Zeballos Fault Zone and the W-MLBA at 47°05′S. At shallow depth, an inferred Pliocene stratified magmatic reservoir (not to scale) located in the Jurassic Ibáñez/El Quemado acid volcanics hosts primitive asthenosphere-derived mafic melts. Then, the studied evolved syenitic and granitic liquids are generated by assimilation–fractional crystallization (AFC) processes from the stored basaltic melts. Major Pliocene structures and stratigraphic units of the study area are shown. See location of profile in Fig. 2a.

lava flows mainly in the eastern edge of the MLBA (Brown et al., 2004; Singer et al., 2004) (Fig. 12).

The initiation of this volcanic event in the western MLBA would have been triggered both by the upward pushing of the sub-slab upwelling mantle and the onset of a new tectonic regime. This would allow the upwelling of magmas to upper crustal levels, storing in recently created spaces and later, together with the effect of lithostatic ice rebound (e.g. Bevis et al., 2006) and high erosional rates (Thomson et al., 2001), the exhumation of the sub-volcanic bodies (see discussion below).

8.3. Implications for the Pliocene tectonic evolution of Patagonia

The area south of LGCBA is located just above the estimated present-day location of the subducted (ca. 6 Ma ago) SCR-1 segment of the South Chile ridge (Cande and Leslie, 1986), then the sub-oceanic plate mantle is in direct contact with the continental mantle wedge (Fig. 1). Our recent work on alkali flood basalts in the region (Espinoza et al., 2005a; Guivel et al., 2006) and that of other workers (Ramos and Kay, 1992; Gorring et al., 1997; Gorring and Kay, 2001; Gorring et al., 2003; among others) clearly indicate the occurrence of a thermal and compositional mantle anomaly below the region since, at least, Eocene times. Furthermore, geophysical surveys in the region (e.g. Murdie et al., 2000) confirm the actual occurrence of this hot mantle anomaly below LGCBA. However, the present (and past) continental response associated to this mantle–lithosphere interaction is still poorly understood, especially regarding possible changes of the tectonic regime.

In other regions where syenitic and alkaline-granite bodies (plus other lithologies) occur jointly, it is common to find them in locally circular arrangements, with ring dykes of different compositions surrounding the main intrusion or crosscutting it (Mingram et al., 2000; Riishuus et al., 2006), but also in linear arrangements (Tchameni et al., 2001; Upadhyay et al., 2006). The latter is generally attributed to a continental rift setting (or transtensional tectonics; Wang et al., 2005), because

in many well-known ancient and actual rift systems (Central Russia, India, East African Rift) alkali intrusions are common and even considered characteristic for this type of geotectonic setting (Litvinovsky et al., 2002; Peccerillo et al., 2003; Upadhyay et al., 2006). In Central Patagonia, these ~3–4 Ma old alkaline intrusions (and rectilinear dykes) outcrop at ca. 1800 m a.s.l. at the top of the western edge of the MLBA, and are aligned along the N160–170 trending lineament of the Zeballos Fault Zone (ZFZ) paralleling the morphotectonic front of one segment of the Patagonian Cordillera (Figs. 2 and 3). All these features could indicate that the process of magma intrusion either benefited from pre-existing structures associated with the Cordilleran construction (pre-~15 Ma; Ramos, 1989; Suárez et al., 2000; Lagabrielle et al., 2004) or occurred during the onset of a new transtensional or extensional Pliocene tectonic event in the region, or both.

Our field observations (intrusive relationships, occurrence of dykes following the major trend of the intrusives; Fig. 3), may indicate ~WE transtensional tectonics that suggest vertical displacement along the Zeballos Fault Zone. Previously described normal and strike-slip faults in the ZFZ support this idea (Lagabrielle et al., 2004, 2006) as well as the evidence of 5–3 Ma old tectonic-controlled paleo-topography at the foot of the main MLBA scarp in the studied region (Lagabrielle et al., submitted for publication) (Fig. 12). Furthermore, the spatial distribution of the intrusives following the ZFZ trace also correlates with a series of N160–170 regional lineaments occurring north and south of LGCBA (Puerto Ibáñez-Chile Chico Fault Zone; Lagabrielle et al., 2004), which in turn coincide with the trend of the subducted Chile Ridge segments (B. Scalabrino, in preparation).

The geodynamic significance of the magmato-tectonic events which occurred in the MLBA between ca. 4–3 Ma is not yet clearly understood. However, we have several lines of evidence that important events occurred at that time in the region. These are of three types: magmatic, tectonic and geodynamic. Magmatic events include: (i) the change from main-plateau alkali basaltic to post-plateau basanitic volcanism, which involved a significant decrease of the partial melting degrees of their mantle sources (Gorring et al., 1997, 2003; Guivel et al., 2006); (ii) the genesis of the studied felsic lavas, and (iii) the occurrence of the Las Nieves pluton (Morata et al., 2002). The tectonic events, which are not so well-constrained in time but occurred after 4 Ma, include (i) the collapse of the central part of the LGCBA region (development of the LGCBA transverse rift zone) leaving relict planar surfaces of Avellanos and Meseta Chile Chico (Lagabrielle et al., 2004; Espinoza et al., 2005b), and (ii) the development of strike-slip faulting along the ZFZ (Lagabrielle et al., 2004, 2006). Finally, at 3 Ma, the main geodynamical event is the collision of the SCR 0 segment with the Chile Trench (Cande and Leslie, 1986). This event affected a region of the Cordillera underlain by a hot and weak mantle due to the presence of the subducted SCR-1 segment migrating progressively northeastwards (Fig. 1). We tentatively propose that the arrival near the trench followed by the collision and the final subduction of segment SCR 0 disturbed the regional tectonic regime and changed drastically the tectonic coupling between the descending oceanic lithosphere and the upper South American plate, south of the Tres Montes Fault Zone (Fig. 1). New structural work and fault data need to be compiled in order to better constrain the regional tectonic aspects of this event.

9. Conclusion

A series of alkaline felsic intrusions, ranging from syeno-diorite to alkali microgranite, together with associated trachytic lava flows, dated between 3.98 and 3.08 Ma, occur in the western flank of the MLBA basaltic plateau. This magmatism occurred synchronously with the emplacement of young mafic lavas on the Meseta (post-plateau basalts), and they are genetically related. The felsic intrusive rocks are aligned along a major N160–170 tectonic corridor (the Zeballos Fault Zone), and crosscut Jurassic volcanics and Miocene sediments. The intrusion benefited from a regional transtensional or extensional tectonics (rift-like) prevailing in the area of LGCBA during the Pliocene, and related to a regional tectonic event that occurred in possible relation with the collision of one segment of the Chile Spreading Ridge with the trench. The Pliocene felsic magmatism in the LGCBA region was initiated when sub-slab asthenospheric basaltic melts ascended through a slab tear/window at ~4–3 Ma (MLBA post-plateau basalts), then part of them were stored at shallow crustal levels in magma chambers hosted by Jurassic ignimbrites. This storing gave opportunity to large-scale fractional crystallization of the mineral phases now observed in the samples (plagioclase, clinopyroxene, Fe–Ti oxides, apatite plus zircon) and to variable degrees of assimilation of the host rock. An AFC model is proposed as the most likely petrogenetic process able to account for the geochemical signature of the studied felsic rocks and to explain their scarcity with respect to coeval basalts.

A-type granitoids are mainly associated with anorogenic to post-orogenic continental settings, and tectonic

processes such as slab breakoff or delamination of a thickened lithosphere are often considered responsible for a hot mantle upwelling (mantle-derived magmas or upwelling asthenosphere) (Whalen et al., 1996) capable to generate the high melting temperatures required for the generation of this type of magmas (Clemens et al., 1986). Furthermore, A_1-type granites (Eby, 1992), which show elemental ratios similar to oceanic island basalts, have been related with the inferred occurrence of hotspot activity related to mantle plumes, generally associated with OIB-type extensive basaltic magmatism or to intraplate rifting. The data presented here show that is possible to generate magmas with A_1-type geochemical characteristics through open-system fractionation processes (AFC) occurring in other geodynamic settings such as back-arc areas, particularly after active ridge subduction.

Acknowledgements

This work is part of the ECOS–CONICYT C05U01 (D.M. and Y.L.) and DyETI—INSU–CNRS (Y.L.) projects. Comments by the Editor N. Eby and detailed revisions by C. Stern and one anonymous reviewer led to improve considerably the manuscript. The authors would like to thank Mr. Marcel Bohn (UMR 6538, Brest, France) for the assistance with the microprobe analyses, Mr. Thierry Aigouy (LMTG, Toulouse, France) for the SEM–EDS analyses, Mr. Pierre Brunet (LMTG, Toulouse, France) for the TIMS measurements and Estancia Sol de Mayo crew (Santa Cruz, Argentina) for the field facilities and hospitality. The first author would also like to thank CONICYT (Chile)–BIRF for providing his PhD fellowship.

References

Ayalew, D., Yirgu, G., 2003. Crustal contribution to the genesis of Ethiopian plateau rhyolitic ignimbrites: basalt and rhyolite geochemical provinciality. Journal of the Geological Society (London) 160, 47–56.

Aries, S., Valladon, M., Polvé, M., Dupré, B., 2000. A routine method for oxide and hydroxide interference corrections in ICP-MS chemical analyses of environmental and geological samples. Geostandards Newsletter 24, 19–31.

Ayers, M., Harris, N., 1997. REE fractionation and Nd-isotope disequilibrium during crustal anatexis: constraints from Himalayan leucogranites. Chemical Geology 139, 249–269.

Baker, P.E., Rea, W.J., Skarmeta, J., Caminos, R., Rex, D.C., 1981. Igneous history of the Andean Cordillera and Patagonian Plateau around latitude 46°S. Philosophical transactions of the Royal Society of London. A 303, 105–149.

Bell, M., Suárez, M., 2000. The Río Lácteo formation of southern Chile. Late Paleozoic orogeny in the Andes of southernmost South America. Journal of South American Earth Science 13, 133–145.

Bellon, H., Quoc Buu, N., Chaumont, J., Philippet, J.C., 1981. Implantation ionique d'argon dans une celibe support: application au tracage isotopique d l'argon contenu dans les minéraux et les roches. Comptes Rendus de l'Académie des Sciences, Paris 292, 977–980.

Benoit, M., Polvé, M., Ceuleneer, G., 1996. Trace element and isotopic characterization of mafic cumulates in a fossil mantle diapir (Oman ophiolite). Chemical Geology 134, 199–214.

Bevis, M.G., Kendrick, E., Zhou, H., Smalley, R., Casassa, G., Parra, H., Lauria, E., 2006. Has the recent tectonic history of Patagonia equipped it with an anomalous viscoelastic response to changing ice loads? Backbone of the Americas, Mendoza (Argentina), 13–7, p. 105.

Brown, L.L., Singer, B.S., Gorring, M.L., 2004. Paleomagnetism and $^{40}Ar/^{39}Ar$ chronology of lavas from Meseta del Lago Buenos Aires, Patagonia. Geochemistry, Geophysical, Geosystem 5 (1), Q01H04. doi:10.1029/2003GC000526.

Bruce, R.M., Nelson, E.P., Weaver, S.G., Lux, D.R., 1991. Temporal and spatial variations in the southern Patagonian batholith; Constraints on magmatic arc development. In: Harmon, R.S., Rapela, C.W. (Eds.), Andean Magmatism and its tectonic setting. Geological Society of America, Special Paper, vol. 265, pp. 1–12.

Busteros, A., y Lapido, O., 1983. Rocas básicas en la vertiente noroccidental de la meseta del lago Buenos Aires, provincial de Santa Cruz. Revista Asociación Geológica Argentina 38 (3–4), 427–436.

Cande, S.C., Leslie, R.B., 1986. Late Cenozoic tectonics of the Southern Chile trench. Journal of Geophysical Research 91, 471–496.

Clemens, J.D., Holloway, J.R., White, A.J.R., 1986. Origin of an A-type granite: experimental constraints. American Mineralogist 71, 317–324.

Cotten, J., Le Dez, A., Bau, M., Caroff, M., Maury, R.C., Dulski, P., Fourcade, S., Bohn, M., Brousse, R., 1995. Origin of anomalous rare-earth elements and yttrium enrichments in subaereally exposed basalts: evidence from French Polynesia. Chemical Geology 119, 115–138.

D'Orazio, M., Agostini, S., Mazzarini, F., Innocenti, F., Manetti, P., Haller, M.J., Lahsen, A., 2000. The Pali Aike volcanic field, Patagonia: slab-window magmatism near the tip of South America. Tectonophysics 321, 407–427.

D'Orazio, M., Agostini, S., Innocenti, F., Haller, M.J., Manetti, P., Mazzarini, F., 2001. Slab window-related magmatism from southernmost South America: the late Miocene mafic volcanics from the Estancia Glencross Area (~52°S Argentina–Chile). Lithos 57, 67–89.

Dasilva, M., Gorring, M.L., Singer, B., Brown, L., 2006. Ridge subduction volcanism in the Zeballos Complex, Southern Patagonian Andes. Backbone of the Americas, Mendoza (Argentina), 4–6, p. 49.

Defant, M.J., Richerson, M., de Boer, J.Z., Stewart, R.H., Maury, R.C., Bellon, H., Drummond, M.S., Feigenson, M.D., Jackson, T.E., 1991. Dacite genesis via both slab melting and differentiation: Petrogenesis of La Yeguada Volcanic Complex, Panama. Journal of Petrology 32, 1101–1142.

DeMets, C., Gordon, R.G., Argus, D.F., Stein, S., 1990. Current plate motions. Geophysics Journal International 101, 425–478.

DePaolo, D.J., 1981. Trace element and isotopic effects of combined wallrock assimilation and fractional crystallization. Earth and Planetary Science Letters 53, 189–202.

Dufek, J., Bergantz, G.W., 2005. Lower crustal magma genesis and preservation: a stochastic framework for the evaluation of basalt–crust interaction. Journal of Petrology 46, 2167–2196.

Eby, G.N., 1992. Chemical subdivision of the A-type granitoids: petrogenetic and tectonic implications. Geology 20, 641–644.

Escosteguy, L., Dal Molin, C., Franchi, M., Geuna, S., Lapido, O., 2002. Estratigrafía de la cuenca de los ríos El Zeballos y Jeinemeni, Noroeste de la provincia de Santa Cruz. XV Congreso Geológico Argentino, El Calafate.

Espinoza, F., Morata, D., Pelleter, E., Maury, R.C., Suárez, M., Lagabrielle, Y., Polvé, M., Bellon, H., Cotten, J., De la Cruz, R., Guivel, C., 2005a. Petrogenesis of the Eocene and Mio-Pliocene alkaline basaltic magmatism in Meseta Chile Chico, Southern Patagonia, Chile: evidence for the participation of two slab windows. Lithos 82, 315–343.

Espinoza, F., Suárez, M., Lagabrielle, Y., Morata, D., Polvé, M., Barbero, L., Maury, R.C., Guivel, C., De la Cruz, R., 2005b. Tectonics in Central Patagonian Cordillera related to Mio-Pliocene subduction on the Chile Ridge: preliminary morphological, chronological and geochemical evidences. 6th International Symposium on Andean Geodynamics—ISAG. Barcelona (España), pp. 250–253.

Faúndez, V., Hervé, F., Lacassie, J.P., 2002. Provenance studies of prelate Jurassic metaturbidite successions of the Patagonian Andes, southern Chile. New Zealand Journal of Geology and Geophysics 45 (4), 411–425.

Flint, S.S., Prior, D.J., Agar, S.M., Turner, P., 1994. Stratigraphic and structural evolution of the Tertiary Cosmelli Basin and its relationship to the Chile triple junction. Journal of the Geological Society (London) 151, 251–268.

Giacosa, R., Franchi, M., 2001. Hojas Geológicas 4772-III y 4772-IV, Lago Belgrano y Lago Posadas. Provincia de Santa Cruz. Instituto de Geología y Recursos Minerales, Servicio Geológico Minero Argentino. Boletín 256. 68 pp. Buenos Aires.

Gieré, R., Sorensen, S., 2004. Allanite and other REE-rich epidote-group minerals. Reviews in Mineralogy and Geochemistry 56, 431–493.

Gorring, M., Kay, S., 2001. Mantle processes and sources of Neogene slab window magmas from southern Patagonia, Argentina. Journal of Petrology 42 (6), 1067–1094.

Gorring, M.L., Kay, S.M., Zeitler, P.K., Ramos, V.A., Rubiolo, D., Fernández, M.I., Panza, J.L., 1997. Neogene Patagonian plateau lavas: continental magmas associated with ridge collision at the Chile Triple Junction. Tectonics 16, 1–17.

Gorring, M., Singer, B., Gowers, J., Kay, S., 2003. Plio-Pleistocene basalts from the Meseta del Lago Buenos Aires, Argentina: evidence for asthenosphere–lithosphere interactions during slab window magmatism. Chemical Geology 193, 215–235.

Gualda, G.A.R., Vlach, S.R.F., 2006. The Serra da Graciosa A-type Granites and Syenites, southern Brazil, Part 2: petrographic and mineralogical evolution of the alkaline and aluminous associations. Lithos 93, 310–327.

Guivel, C., Morata, D., Pelleter, E., Espinoza, F., Maury, R.C., Lagabrielle, Y., Polvé, M., Bellon, H., Cotten, J., Benoit, M., Suárez, M., De la Cruz, R., 2006. Miocene to Late Quaternary Patagonian basalts (46–47°S): geochronometric and geochemical evidence for slab tearing due to active spreading ridge subduction. Journal of Volcanology and Geothermal Research 149, 346–370.

Hashimoto, S., Fujiwara, Y., Nishimura, T., 1977. Olivine basalt in the north-western part of the Patagonia, Argentina. In: Ishikawa, T., Aguirre, L. (Eds.), Comparative studies on the geology of the circum Pacific orogenic belts. Japan Society for the Promotion of Science, pp. 161–175.

Hawkesworth, C.J., Norry, M.J., Roddick, J.C., Baker, P.E., Francis, P.W., Thorpe, R.S., 1979. $^{143}Nd/^{144}Nd$, $^{87}Sr/^{86}Sr$ and incompatible trace element variations in calc-alkaline andesitic and plateau lavas from South America. Earth Planetary Science Letters 42, 45–57.

Hervé, F., Aguirre, L., Godoy, E., Massone, H.-J., Morata, D., Pankhurst, R.J., Ramírez, E., Sepú lveda, V., Willner, A., 1998. Nuevos antecedentes acerca de la edad y las condiciones P–T de los Complejos Metamórficos en Aysén, Chile. X Congreso Latinoamericano de Geología, Buenos. Aires (Argentina), pp. 134–137.

Hervé, F., Demant, A., Ramos, V.A., Pankhurst, R.J., Suárez, M., 2000. The southern Andes. In: Cordani, U.G., Milani, E.J., Thomaz Filho, A., Campos, D.A. (Eds.), Tectonic Evolution of South America. 31th International Geological Congress, Rio de Janeiro (Brazil), pp. 605–634.

Hervé, F., Pankhurst, R.J., Fanning, C.M., Calderón, M., Yaxley, G.M., 2007. The South Patagonian Batholith: 150 my of granite magmatism on a plate margin. Lithos 97, 373–394.

Hole, M.J., Saunders, A.D., Rogers, G., Sykes, M.A., 1995. The relationship between alkaline magmatism, lithospheric extension and slab window formation along continental destructive plate margins. In: Smellie, J.L. (Ed.), Volcanism Associated with Extension at Consuming Plate Margins. Geological Society of London Special Publication, vol. 81, pp. 265–285.

Introcaso, A., Pacino, M.C., Guspi, F., 1996. The Argentina–Chile Andes, Crustal thickness, isostasy, shortening and anomaly prediction from gravity studies. 3rd International Symposium on Andean Geodynamics, St Malo (France).

Irvine, T.N., Baragar, W.R.A., 1971. A guide to the chemical classification of the common volcanic rocks. Canadian Journal of Earth Science 8, 523–548.

Kilian, R., Behrmann, J., 2003. Geochemical constraints on the sources of southern Chile Trench sediments and their recycling in arc magmas of the Southern Andes. Journal of the Geological Society (London) 160, 57–70.

Lagabrielle, Y., Suárez, M., Rosselló, E.A., Hérail, G., Martinod, J., Régnier, M., de la Cruz, R., 2004. Neogene to Quaternary tectonic evolution of the Patagonian Andes at the latitude of the Chile triple junction. Tectonophysics 385, 211–241.

Lagabrielle, Y., Bellon, H., Espinoza, F., Guivel, C., Malavieille, J., Maury, R., Morata, D., Polvé, M., Rosselló, E., Suárez, M., 2006. Post-Pliocene deformation and uplift of the Patagonian Andes in response to the subduction of the active Chile spreading ridge (CSR). Backbone of the Americas, Mendoza (Argentina), 4–2, p. 47.

Lagabrielle, Y., Suárez, M., Malavieille, J., Morata, D., Espinoza, F., Maury, R.C., Scalabrino, B., Barbero, L., De la Cruz, R., Rosselló, E., Bellon, H., submitted for publication. Pliocene extensional tectonics in Eastern Central Patagonian Cordillera: geochronological constraints and new field evidence. Terra Nova.

Le Bas, M.J., Le Maitre, R.W., Streckeisen, A., Zanettin, B., 1986. A chemical classification of volcanic rocks based on the total alkali–silica diagram. Journal of Petrology 27, 745–750.

Litvinovsky, A.A., Jahn, B.M., Zanvilevich, A.N., Saunders, A., Poulain, S., Kuzmin, D.V., Reichow, M.K., Titov, A.V., 2002. Petrogenesis of syenite-granite suites from the Bryansky Complex (Transbaikalia, Russia): implications for the origin of A-type granitois magmas. Chemical Geology 189, 105–133.

Mahood, G., Drake, R.E., 1982. K–Ar dating young rhyolitic rocks: a case study for the Sierra La Primavera, Jalisco, México. Geological Society of America Bulletin 93, 1232–1241.

Marks, M., Markl, G., 2001. Fractionation and assimilation processes in the alkaline augite syenite unit of the Ilímaussaq Intrusion, South Greenland, as deduced from phase equilibria. Journal of Petrology 42 (10), 1947–1969.

Marshall, L.G., Salinas, P., 1990. Stratigraphy of the Río Frías formation (Miocene), along the Alto Río Cisnes, Aysén, Chile. Revista Geológica de Chile 17, 57–88.

Middlemost, E.A.K., 1975. The basalt clan. Earth Sciences Review 11, 337–364.

Mingram, B., Trumbull, R.B., Littman, S., Gerstenberger, H., 2000. A petrogenetic study of androgenic felsic magmatism in the Cretaceous Paresis ring complex, Namibia: evidence for mixing of crust and mantle-derived components. Lithos 54, 1–22.

Morata, D., Barbero, L., Suárez, M., De La Cruz, R., 2002. Early Pliocene magmatism and high exhumation rates in the Patagonian Cordillera (46°40′S) K–Ar and fission track data. 5th International Symposium on Andean Geodynamics (ISAG), Toulouse, France, pp. 433–436.

Morimoto, N., Fabries, J., Ferguson, A.K., Ginzburg, I.V., Ross, M., Seifert, F.A., Zussmann, J., Aoki, K., Gottardi, G., 1988. Nomenclature of pyroxenes. American Mineralogist 173, 1123–1133.

Murdie, R., Styles, P., Prior, D.J., Daniel, A.J., 2000. A new gravity map of southern Chile and its preliminary interpretation. Revista Geológica de Chile 27 (1), 49–63.

Nakamura, N., 1974. Determination of REE, Ba, Fe, Mg, Na and K in carbonaceous and ordinary chondrites. Geochimica et Cosmochimica Acta 38, 757–775.

Pankhurst, R.J., Leat, P.T., Sruoga, P., Rapela, C.W., Márquez, M., Storey, B.C., Riley, T.R., 1998. The Chon Aike province of Patagonia and related rocks in West Antarctica: a silicic large igneous province. Journal of Volcanology and Geothermal Research 81, 113–136.

Parada, M.A., Lahsen, A., Palacios, C., 2001. Ages and geochemistry of Mesozoic–Eocene back-arc volcanic rocks in the Aysén region of the Patagonian Andes, Chile. Revista Geológica de Chile 28 (1), 25–46.

Pearce, J.A., Harris, N.B.W., Tindle, A.G., 1984. Trace element discrimination diagrams for the tectonic interpretation of granitic rocks. Journal of Petrology 25, 956–983.

Peccerillo, A., Barberio, M.R., Yirgu, G., Ayalew, D., Barbieri, M., Wu, T.W., 2003. Relationships between mafic and peralkaline silicic magmatism in continental rift settings: a petrological, geochemical and isotopic study of the Gedesma Volcano, Central Ethiopian Rift. Journal of Petrology 44 (11), 2003–2032.

Pin, C., Telouk, P., Imbert, J.-L., 1995. Direct determination of the samarium: neodymium ratio in geological materials by inductively coupled plasma quadrupole mass spectrometry with cryogenic desolvation. Comparison with isotope dilution thermal ionization mass spectrometry. Journal of Analytical Atomic Spectrometry 10, 93–98. doi:10.1039/JA9951000093.

Poitrasson, F., 2002. In situ investigation of allanite hydrothermal alteration: examples from calc-alkaline and anorogenic granites of Corsica (southeast France). Contributions to Mineralogy and Petrology 142, 485–500.

Ramos, V.A., 1989. Andean foothills structures in northern Magallanes Basin, Argentina. American Association of Petroleum Geologist Bulletin 73, 887–903.

Ramos, V.A., Kay, S.M., 1992. Southern Patagonian Plateau basalts and deformation: backarc testimony of ridge collision. Tectonophysics 205, 261–282.

Riishuus, M.S., Peate, D.W., Tegner, C., Wilson, J.R., Brooks, C.K., Harris, C., 2006. Temporal evolution of a long-lived syenitic centre: the Kangerlussuaq Alkaline Complex, East Greenland. Lithos 92 (1–2), 276–299.

Schmidt, M.W., Poli, R., 1998. Experimentally based water budgets for dehydrating slabs and consequences for arc magma generation. Earth Planetary Science Letters 163, 361–379.

Shinjo, R., Kato, Y., 2000. Geochemical constraints on the origin of bimodal magmatism in the Okinawa Trough, an incipient backarc basin. Lithos 54, 117–137.

Singer, B.S., Ackert Jr., R.P., Guillou, H., 2004. $^{40}Ar/^{39}Ar$ and K–Ar chronology of Pleistocene glaciations in Patagonia. Geological Society of America Bulletin 116, 434–450. doi:10.1130/B25177.1.

Steiger, R.H., Jäger, E., 1977. Subcommission on geochronology: convention on the use of decay constants in geo- and cosmochronology. Earth and Planetary Science Letters 36, 359–362.

Stern, C.R., 1999. Black obsidian from central-south Patagonia: chemical characteristics, sources and regional distribution of artifacts. In: Goni, R. (Ed.), Soplando en el veinto: Avances en la arqueologia de la Patagonia. Publicación del Centro Nacional Patagónico, Puerto Madryn (Argentina), pp. 221–234.

Stern, C.R., 2004. Obsidian source and distribution in southernmost Patagonia: review of the current information. In: Civalero, M.T., Guraieb, A., Fernandez, R. (Eds.), Contra viento y marea: arqueología de Patagonia. Miramar Publishing, Buenos Aires (Argentina), pp. 167–178.

Stern, C.R., Frey, F.A., Futa, K., Zartman, R.E., Peng, Z., Kyser, T.K., 1990. Trace-element and Sr, Nd, Pb and O isotopic composition of Pliocene and Quaternary basalts of the Patagonian Plateau Lavas of southernmost South America. Contributions to Mineralogy and Petrology 104, 294–308.

Stevenson, R., Upton, B.G.J., Steenfelt, A., 1997. Crust–mantle interaction in the evolution of the Ilímaussaq Complex, South Greenland: Nd isotopic studies. Lithos 40, 189–202.

Suárez, M., De La Cruz, R., Bell, C.M., 2000. Timing and origin of deformation along the Patagonian fold and thrust belt. Geological Magazine 137, 345–353.

Sun, S., McDonough, W.F., 1989. Chemical and isotopic systematics of oceanic basalts; implications for mantle composition and processes. In: Saunders, A.D., Norry, J.M. (Eds.), Magmatism in the Ocean Basins. Geological Society of London Special Publication, vol. 42, pp. 313–345.

Tassara, A., Götze, H.-J., Schmidt, S., Hackney, R., 2006. Three-dimensional density model of the Nazca plate and the Andean continental margin. Journal of Geophysical Research 111, B09404. doi:10.1029/2005JB003976.

Tchameni, R., Mezger, K., Nsifa, N.E., Pouclet, A., 2001. Crustal origin of early Proterozoic syenites in the Congo Craton (Ntem Complex), South Cameroon. Lithos 57, 3–42.

Thomson, S.N., Hervé, F., Stöckhert, B., 2001. Mesozoic–Cenozoic denudation history of the Patagonian Andes (southern Chile) and its correlation to different subduction processes. Tectonics 20, 693–711.

Thorkelson, D.J., Breitsprecher, K., 2005. Partial melting of slab window margins: genesis of adakitic and non-adakitic magmas. Lithos 79, 25–41.

Ton-That, T., Singer, B., Mörner, N.A., Rabassa, J., 1999. Datación de lavas basálticas por $^{40}Ar/^{39}Ar$ y geología glacial de la región del lago Bueno Aires, provincia de Santa Cruz, Argentina. Revista de la Asociación Geológica Argentina 54, 333–352.

Trua, T., Deniel, C., Mazzuoli, R., 1999. Crustal Control in the genesis of Plio-Quaternary bimodal magmatism of the Ethiopian Rift (MER): geochemical and isotopic (Sr, Nd, Pb) evidence. Chemical Geology 155, 201–231.

Turner, J.S., Campbell, I.H., 1986. Convection and mixing in magma chambers. Earth-Science Reviews 23, 255–352.

Ugarte, F., 1956. El Grupo Río Zeballos. Revista de la Asociación Geológica Argentina 11 (3), 202–216.

Upadhyay, D., Raith, M.M., Mezger, K., Hammerschmidt, K., 2006. Mesoproterozoic rift-related alkaline magmatism at Elchuru, Prakasam Alkaline Province, SE India. Lithos 89, 447–477.

Vernikovsky, V.A., Pease, V.L., Vernikovskaya, A.E., Romanov, A.P., Gee, D.G., Travin, A.V., 2003. First report of early Triassic A-type granite and syenite intrusions from Taimyr: product of the northern Eurasian superplume? Lithos 66, 23–36.

Wang, Q., Li, J.W., Jian, P., Zhao, Z.H., Xiong, X.L., Bao, Z.W., Xu, J.F., Li, C.F., Ma, J.L., 2005. Alkaline syenites in eastern Cathaysia (South China): link to Permian–Triassic transtension. Earth and Planetary Science Letters 230, 339–354.

Weaver, S.G., Bruce, R., Nelson, E.P., Brueckner, H.K., Lehuray, A.P., 1990. The Patagonian batholith at 48° S latitude, Chile: geochemical and isotopic variations. In: Kay, S.M., Rapela, C.W. (Eds.), Plutonism from Antarctica to Alaska. Geological Society of America Special Paper, vol. 241, pp. 33–50.

Wedepohl, K.H., Hartmann, G., 1994. The composition of the primitive upper earth's mantle. In: Meyer, H.O.A., Leonardos, O.H. (Eds.), Kimberlites, related rocks and mantle xenoliths. Companhia de Pesquisa de Recursos Minerais, Rio de Janeiro (Brazil), vol. 1, pp. 486–495.

Whalen, J.B., Currie, K.L., Chappell, B.W., 1987. A-type granites: geochemical characteristics, discrimination and petrogenesis. Contributions to Mineralogy and Petrology 95, 407–419.

Whalen, J.B., Jenner, G.A., Longstaffe, F.J., Robert, F., Gariepy, C., 1996. Geochemical and isotopic (O, Nd, Pb and Sr) constraints on A-type granite: petrogenesis based on the Topsails igneous suite, Newfoundland Appalachians. Journal of Petrology 37, 1463–1489.